

*Cy. 83*

## Experimental Study of Plastic Responses of Pipe Elbows

W. L. Greenstreet

Prepared for the U.S. Nuclear Regulatory Commission  
Office of Nuclear Regulatory Research  
Under Interagency Agreements ERDA 40-551-75 and 40-552-75

OAK RIDGE NATIONAL LABORATORY  
CENTRAL RESEARCH LIBRARY  
DOCUMENT COLLECTION

**LIBRARY LOAN COPY**

DO NOT TRANSFER TO ANOTHER PERSON

If you wish someone else to see this  
document, send in name with document  
and the library will arrange a loan.

UCN-7369  
(3-67)

**OAK RIDGE NATIONAL LABORATORY**  
OPERATED BY UNION CARBIDE CORPORATION - FOR THE DEPARTMENT OF ENERGY

Printed in the United States of America. Available from  
National Technical Information Service  
U.S. Department of Commerce  
5285 Port Royal Road, Springfield, Virginia 22161  
Price: Printed Copy \$5.25; Microfiche \$3.00

This report was prepared as an account of work sponsored by an agency of the United States Government. Neither the United States Government nor any agency thereof, nor any of their employees, contractors, subcontractors, or their employees, makes any warranty, express or implied, nor assumes any legal liability or responsibility for any third party's use or the results of such use of any information, apparatus, product or process disclosed in this report, nor represents that its use by such third party would not infringe privately owned rights.

ORNL/NUREG-24  
Dist. Category NRC-5

Contract No. W-7405-eng-26

Engineering Technology Division

EXPERIMENTAL STUDY OF PLASTIC RESPONSES  
OF PIPE ELBOWS

W. L. Greenstreet

Manuscript completed -- January 20, 1978

Date Published: February 1978

Prepared for the  
U.S. Nuclear Regulatory Commission  
Office of Nuclear Regulatory Research  
under Interagency Agreements  
ERDA 40-551-75 and 40-552-75

Prepared by the  
OAK RIDGE NATIONAL LABORATORY  
Oak Ridge, Tennessee 37830  
operated by  
UNION CARBIDE CORPORATION  
for the  
DEPARTMENT OF ENERGY



## CONTENTS

	<u>Page</u>
FOREWORD . . . . .	v
ABSTRACT . . . . .	1
INTRODUCTION . . . . .	1
DESCRIPTION OF SPECIMENS AND TESTS . . . . .	3
EXPERIMENTAL RESULTS . . . . .	15
INTERPRETATION OF RESULTS . . . . .	35
CONCLUSIONS . . . . .	47
ACKNOWLEDGMENT . . . . .	48
REFERENCES . . . . .	48
APPENDIX: DIMENSIONAL DATA FOR SPECIMENS PE-17 THROUGH -20 . . .	51



## FOREWORD

This work was performed at the Oak Ridge National Laboratory (ORNL) in support of the ORNL Design Criteria for Piping and Nozzles Program being conducted for the U.S. Nuclear Regulatory Commission (USNRC), Office of Nuclear Regulatory Research. E. K. Lynn of the Metallurgy and Materials Branch, Division of Reactor Safety Research, USNRC, is the cognizant engineer, and S. E. Moore of ORNL Engineering Technology Division is the program manager.

The objectives of the ORNL program are to conduct integrated experimental and analytical stress analysis studies of piping system components and pressure vessel nozzles to confirm and/or improve the adequacy of structural design criteria and analytical methods used to assure that nuclear power plants are designed for safe operation. Program activities are coordinated with other safety-related piping and pressure vessel research through the Design Division, Pressure Vessel Research Committee (PVRC) of the Welding Research Council, and through the ASME Boiler and Pressure Vessel Code committees. Results from the ORNL program are used by appropriate codes and standards groups in drafting new or improved design rules and criteria.

The following reports have been issued under U.S. Nuclear Regulatory Commission sponsorship:

J. W. Bryson, J. P. Callahan, and R. C. Gwaltney, *Stress Analyses of Flat Plates with Attached Nozzles, Vol. 1. Comparison of Stresses in a One-Nozzle-to-Flat-Plate Configuration and in a Two-Nozzle Configuration with Theoretical Predictions*, ORNL-5044 (July 1975).

R. L. Battiste et al., *Stress Analysis of Flat Plates with Attached Nozzles, Vol. 2. Experimental Stress Analyses of a Flat Plate with One Nozzle Attached*, ORNL-5044 (July 1975).

E. C. Rodabaugh and S. E. Moore, *Stress Indices for ANSI Standard B16.11 Socket-Welding Fittings*, ORNL/TM-4929 (August 1975).

R. C. Gwaltney, J. W. Bryson, and S. E. Bolt, *Theoretical and Experimental Stress Analyses of ORNL Thin-Shell Cylinder-to-Cylinder Model 2*, ORNL-5021 (October 1975).

S. E. Moore, "Contributions of the ORNL Piping Program to Nuclear Piping Design Codes and Standards," *Proceedings of the Technology Information Meeting on Methods for Analyzing Piping Integrity*, Nov. 11-12, 1975, ERDA-76-50; also in *J. Press. Vessel Technol.*, *Trans. ASME* 99, 224-30 (February 1977).

W. L. Greenstreet, "Summary and Accomplishments of the ORNL Program for Nuclear Piping Design Criteria," *Proceedings of the Technology Information Meeting on Methods for Analyzing Piping Integrity*, Nov. 11-12, 1975, ERDA-76-50.

J. W. Bryson and W. F. Swinson, *Stress Analyses of Flat Plates with Attached Nozzles, Vol. 3. Experimental Stress Analyses of a Flat Plate with Two Closely Spaced Nozzles of Equal Diameter Attached*, ORNL-5044 (December 1975).

E. C. Rodabaugh, F. M. O'Hara, Jr., and S. E. Moore, *FLANGE: A Computer Program for the Analysis of Flanged Joints with Ring-Type Gaskets*, ORNL-5035 (January 1976).

R. E. Textor, *User's Guide for SHFA: Steady-State Heat Flow Analysis of Tee Joints by the Finite Element Method*, UCCND/CSD/INF-60, Oak Ridge Gaseous Diffusion Plant (January 1976).

E. C. Rodabaugh and S. E. Moore, *Flanged Joints with Contact Outside the Bolt Circle - ASME Part B Design Rules*, ORNL/Sub/2913-1, Battelle-Columbus Laboratories (May 1976).

E. C. Rodabaugh, *Appropriate Nominal Stresses for Use with ASME Code Pressure-Loading Stress Indices for Nozzles*, ORNL/Sub/2913-2, Battelle-Columbus Laboratories (June 1976).

S. E. Moore and J. W. Bryson, *Progress Report for the Design Criteria for Piping and Nozzles Program for the Two Quarterly Periods July 1 to Sept. 30 and Oct. 1 to Dec. 31, 1975*, ORNL/NUREG/TM-18 (June 1976).

R. L. Maxwell and R. W. Holland, *Experimental Stress Analysis of the Attachment Region of a Hemispherical Shell with a Radially Attached Nozzle, Zero Penetration*, ORNL/Sub/2203-4, University of Tennessee (July 1976).

J. P. Callahan and J. W. Bryson, *Stress Analyses of Perforated Flat Plates Under In-Plane Loadings*, ORNL/NUREG-2 (August 1976).

E. C. Rodabaugh and S. E. Moore, *Evaluation of the Bolting and Flanges of ANSI B16.5 Flanged Joints - ASME Part A Flanges*, ORNL/Sub/2913-3, Battelle-Columbus Laboratories (September 1976).

E. C. Rodabaugh and R. C. Gwaltney, *Elastic Stresses at Reinforced Nozzles in Spherical Shells with Pressure and Moment Loading*, ORNL/Sub/2913-4, Battelle-Columbus Laboratories (October 1976).

E. C. Rodabaugh, S. E. Moore, and J. N. Robinson, *Dimensional Control of Buttwelding Pipe Fittings for Nuclear Power Plant Class 1 Piping Systems*, ORNL/Sub/2913-5, Battelle-Columbus Laboratories (December 1976).

S. E. Moore and J. W. Bryson, *Design Criteria for Piping and Nozzles Program Quarterly Progress Report for April-June 1976*, ORNL/NUREG/TM-107 (April 1977).

E. C. Rodabaugh and S. E. Moore, *Flexibility Factors for Small ( $d/D < 1/3$ ) Branch Connections with External Loadings*, ORNL/Sub/2913-6, Battelle-Columbus Laboratories (March 1977).

S. E. Moore and J. W. Bryson, *Design Criteria for Piping and Nozzles Program Quarterly Progress Report for July-September 1976*, ORNL/NUREG/TM-91 (February 1977).

P. G. Fowler and J. W. Bryson, *User's Manual for the CORTES Graphics Package GRFPAK*, ORNL/NUREG/TM-127 (August 1977).

B. R. Bass, J. W. Bryson, and S. E. Moore, "Validation of the Finite Element Stress Analysis Computer Program CORTES-SA for Analyzing Piping Tees and Pressure Vessel Nozzles," *Pressure Vessels and Piping Computer Program Evaluation and Qualification*, PVP-PB-024, pp. 9-25, ASME (1977).

J. K. Hayes and S. E. Moore, "Experimental Stress Analysis for Four 24-in. ANSI Standard B16.9 Tees," Paper 77-PVP-4, presented at the ASME Energy Technology Conference and Exhibition, Houston, Tex., Sept. 18-23, 1977.

J. W. Bryson, W. G. Johnson, and B. R. Bass, *Stresses in Reinforced Nozzle-Cylinder Attachments Under Internal Pressure Loading Analyzed by the Finite-Element Method -- A Parameter Study*, ORNL/NUREG-4 (October 1977).

F. K. W. Tso et al., *Stress Analysis of Cylindrical Pressure Vessels with Closely Spaced Nozzles by the Finite-Element Method, Vol. 1. Stress Analysis of Vessels with Two Closely Spaced Nozzles Under Internal Pressure*, ORNL/NUREG-18/V1 (November 1977).



# EXPERIMENTAL STUDY OF PLASTIC RESPONSES OF PIPE ELBOWS

W. L. Greenstreet

## ABSTRACT

Load-deflection responses were determined experimentally for sixteen 152.4-mm (6-in.) (nominal) commercial carbon steel pipe elbows and four 152.4-mm (6-in.) stainless steel elbows. Each specimen was loaded with an external force of sufficient magnitude to produce predominantly plastic response. The influences of bend radius and wall thickness were studied, as well as the effect of internal pressure on load-deflection behavior. Comparisons of results from stainless steel and from carbon steel elbows indicate differences in responses attributable to material differences. The results were interpreted in terms of limit analysis concepts, and collapse loads were determined. Trends given by the collapse loads are identified and discussed.

## INTRODUCTION

This report is concerned with the structural behavior of pipe elbows. These commonly used components are of particular importance because they are often the most flexible members in a piping system and hence are forced to accommodate disproportionate displacements arising from differential movements. In practice, this flexibility is needed to keep the overall forces and stresses in the system within acceptable ranges. However, precautions must be taken to avoid exceeding the range of predominantly elastic response because the resistance to deformation will decrease rapidly with increasing load and may result in malfunction or failure of the component and of the system.

In order to avoid these undesirable structural responses, plastic limit analysis concepts are used for establishing allowable loads. Limit analyses provide estimates of plastic collapse loads, that is, loads above which large increases in deformation result from small increases in load. These large deformations are associated with plastic flow, which dominates to such an extent that the elastic portions of the material do not play a significant role in resisting the deformations. Although these concepts are associated with idealized behaviors adopted for use in mathematical

analyses, they can be applied to structures such as elbows provided that<sup>1</sup>

1. excessive deformations occur before the influence of strain hardening becomes appreciable;
2. changes in geometry of the structure produced by the deflections have negligible effect on the load required to continue the deformation.

Experimentally determined plastic collapse loads are given in this report for 20 commercial short- and long-radius butt-welding elbows, nominally 152.4 mm (6 in.) in diameter. These elbows were loaded by external forces and by combinations of external force and internal pressure. Deflections and strains were measured by means of dial indicators and strain gages, respectively. The dial-indicator readings were the primary sources for limit-load determinations, and the strain-gage data were used for checking purposes and to provide details on the plastic collapse process.

The principal objective of this series of tests was to obtain in-plane and out-of-plane limit moments. The imposed moments were produced by forces acting on moment arms sufficiently long to give essentially only moment loads on the elbows. The specimens were not examined to provide quantitative information regarding the locations and extents of the plastic zones developed or to determine the order in which such zones were formed. However, qualitative data regarding plastic zone location for selected regions were obtained in a few instances.

The test specimens and the experimental procedures are described in the following sections. Representative load-deflection and load-strain curves are included to indicate the results obtained, and the method used for limit-load determination is explained. The limit loads are tabulated, and conclusions regarding the test results are presented.

Results from the first 15 elbow tests were given in Ref. 2. In this report, the contents are expanded to cover results from 5 additional tests, and the overall results are interpreted on the broader bases afforded by the added information.

## DESCRIPTION OF SPECIMENS AND TESTS

A series of room-temperature limit-load tests was conducted on twenty 152.4-mm (6-in.) commercial butt-welding elbows. Sixteen were made from ASTM A-106 grade B carbon steel, and four were made from ASTM A-312 type 304L stainless steel. Short- and long-radius sched-40 and -80 elbows were used. The first 16 were obtained from the same manufacturer; all types are listed in Table 1 along with the nominal dimensions and materials properties. A typical specimen is shown in Fig. 1.

Both types of elbows were made using standard manufacturing procedures. The carbon steel elbows were formed by forcing ASTM A-106, grade B, hot-finished seamless pipe over a mandrel in a furnace where the metal temperature was held within the approximate range of 871 to 982°C (1600 to 1800°F). The formed pieces were then maintained at temperatures in the range quoted and inserted in sizing dies which are used to ensure conformance with the dimensional requirements of ANSI B16.9 and B16.28. Following the forming and sizing operations, the elbows were cooled in still air. The temperatures during fabrication and the method of cooling are in accord with the requirements of ASTM A-234, which does not require that further heat treatment be applied.

The stainless steel elbows were formed by forcing ASTM A-312 type 304L stainless steel seamless pipe through a die cavity at room temperature. An inside mandrel was used in this operation to guide the pipe and to prevent buckling during the forming process. Following fabrication, the elbows were annealed at 1066°C (1950°F) and water quenched.

The materials properties listed in Table 1 were obtained mainly from tensile specimens taken from selected elbows after they were tested. In some cases, specimens were taken from duplicate elbows; the first 16 elbows were from 4 lots, and one from each lot was used. The coupons for the tensile specimens were removed from the outside near the loaded end of each elbow; this region was subjected to relatively low strains during test in all cases. Tensile specimens from each of the last four specimens were tested.

The tensile specimens had a 3.18-mm-diam (0.125-in.), 12.7-mm-long (1/2-in.) gage section and were instrumented with two metallic-foil

Table 1. Nominal dimensions and materials properties of 6-in. elbows used in limit-load tests<sup>a</sup>

Specimens	Description <sup>b</sup>	Nominal dimensions				Specimen material	Lot No.	Modulus of elasticity (psi × 10 <sup>-6</sup> )	0.2% offset yield stress (psi)	Proportional limit yield stress (psi)	Tensile strength (psi)
		D <sub>o</sub> (in.)	D <sub>i</sub> (in.)	D <sub>t</sub> (in.)	D <sub>i</sub> /t						
PE-1 to -6	Sched-40 LR	6.625	6.065	0.280	21.66	ASTM A-106 grade B	S4401	30.1	50,000		73,600
PE-7 to -9	Sched-80 LR	6.625	5.761	0.432	13.34	ASTM A-106 grade B	S3147	30.2	37,800		65,000
PE-10 to -14	Sched-40 SR	6.625	6.065	0.280	21.66	ASTM A-106 grade B	S4521	31.3	39,600		74,100
PE-15, -16	Sched-40 LR	6.625	6.065	0.280	21.66	ASTM A-312 type 304L SS	SPFM	28.8	37,700	13,500	87,800
PE-17	Sched-40 SR	6.625	6.065	0.280	21.66	ASTM A-312 type 304L SS	14247 SSGW	29.8	35,600	16,000	96,600
PE-18	Sched-80 LR	6.625	5.761	0.432	13.34	ASTM A-312 type 304L SS	15526 SSAV	29.7	35,400	18,000	88,100
PE-19	Sched-40 SR	6.625	6.065	0.280	21.66	ASTM A-106 grade B	Heat No. N51382	33.0	46,000		68,000
PE-20	Sched-80 SR	6.625	5.761	0.432	13.34	ASTM A-106 grade B		28.4	34,600		70,400

<sup>a</sup>1 in. = 2.54 × 10<sup>-2</sup> m; 1 psi = 6.895 × 10<sup>3</sup> Pa.

<sup>b</sup>SR = short radius; LR = long radius.

PHOTO 78241



Fig. 1. Typical 25.4-mm (6-in.) long-radius, carbon steel butt-welding elbow.

electrical resistance strain gages having a 6.35-mm (1/4-in.) gage length, except for elbows 17 through 20, which had a gage length of 3.18 mm (1/8 in.). The gages were mounted on opposite sides of the specimen with an epoxy adhesive and connected in series to average the strains. The platen rate was 0.051 mm/min (0.002 in.). Three tensile specimens were tested for lot S4401 (see Table 1) and elbows 17, 18, and 19; two tensile specimens were tested from lot SPFM and five for elbow 20. Average values are given in the table.

Pipe extensions of ASTM A-106 grade B carbon steel of the same thickness as the elbow being tested were welded by the tungsten-arc inert-gas method to the ends of the elbows. Elbow PE-18 was an exception in that 347 stainless steel extensions were used. The assemblies were not heat treated following the welding operations, thus simulating metal conditions to be found in actual piping systems. One extension was then rigidly mounted on a pedestal attached to a load frame. A test setup is shown diagrammatically in Fig. 2. A single force loading was applied in each case, with the point of load application on the free extension at a distance of four to five pipe diameters from the nearer end of the elbow. The loadings of interest were the moments at that end of the elbow; by selecting a relatively long moment arm, the shear forces were small in comparison with the moments. The distance from the other end of the elbow to the plane of restraint (the top of the pedestal on the load frame) was about three pipe diameters.

The specimen numbers, wall thicknesses, bend radii, and loading conditions are listed in Table 2. For the specimens used, a bend radius of 152.4 mm (6 in.) is termed short radius; 228.6 mm (9 in.) is long radius. In cases where the elbows were also internally pressurized, the specimens were held at the design pressure of 10.34 MPa (1500 psi) throughout the test period. The moment sign convention is shown in Fig. 3.

The locations of the dial indicators used to measure deflections for 15 of the 16 carbon steel elbows and 3 of the 4 stainless steel elbows are indicated in Fig. 2. For carbon steel elbow PE-20, dial indicator DI 1 was at 254 mm (10 in.) and dial indicator DI 2 was at 381 mm (15 in.) from the end of the elbow. In the case of stainless steel elbow PE-15, two dial indicators in addition to those shown in Fig. 2 were used to

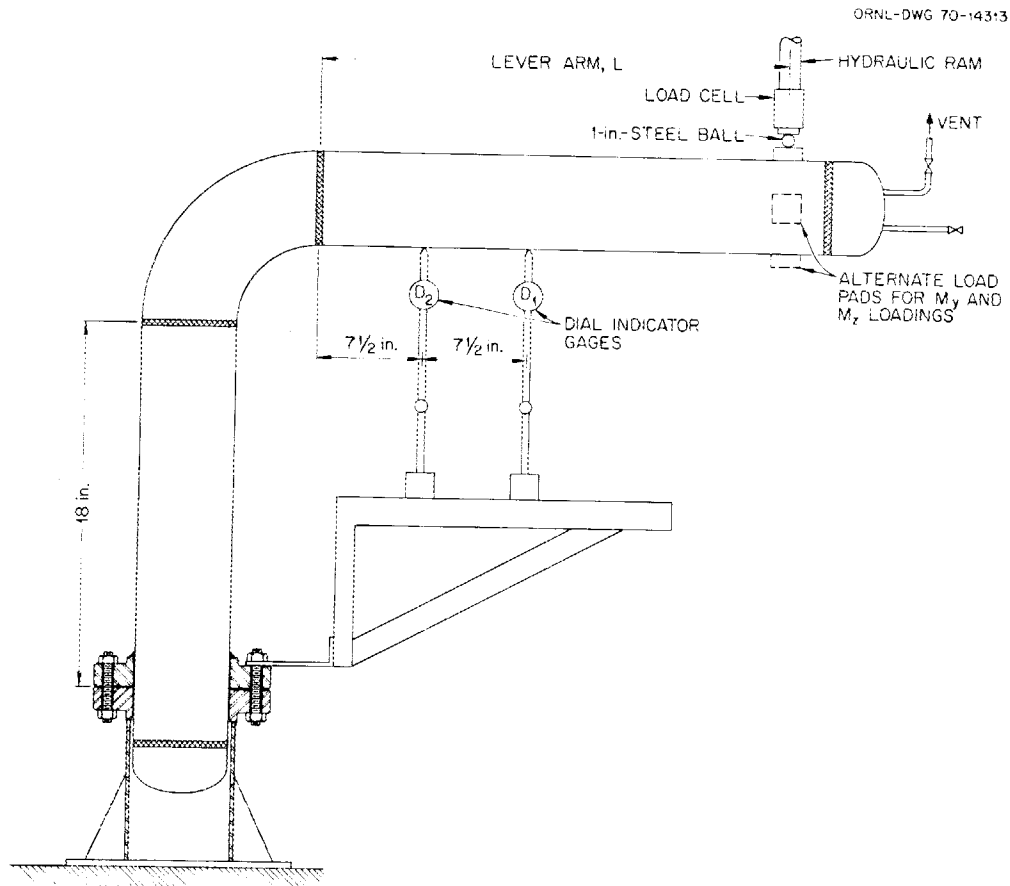


Fig. 2. Diagram of test setup (1 in. = 25.4 mm).

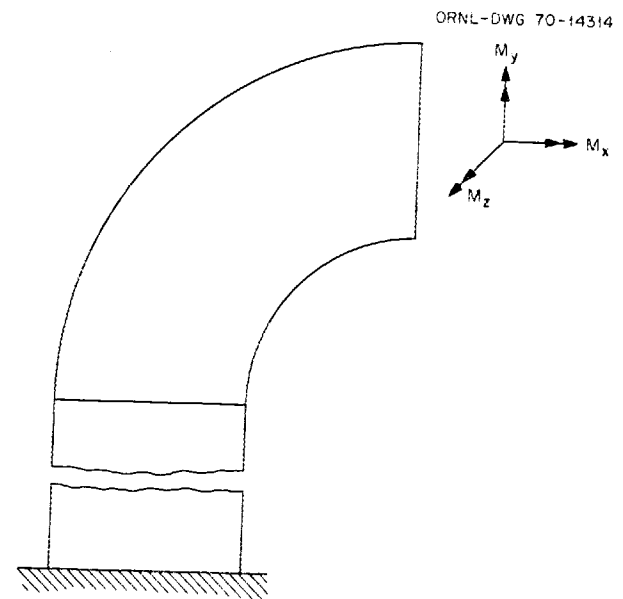


Fig. 3. Diagram of moment sign convention.

Table 2. Plastic limit load tests on 6-in. elbows<sup>a</sup>

Number <sup>b</sup>	Elbow		Loading conditions			
			Moment <sup>c</sup>		Pressure, P	
	Wall thickness (schedule)	Bend radius (in.)	In plane <sup>d</sup>			Out of plane
			+M <sub>z</sub>	-M <sub>z</sub>	M <sub>y</sub>	
PE-1	40	9	X			
PE-2	40	9		X		
PE-3	40	9			X	
PE-4	40	9	X			X
PE-5	40	9		X		X
PE-6	40	9			X	X
PE-7	80	9	X			
PE-8	80	9		X		
PE-9	80	9			X	
PE-10	40	6	X			
PE-11	40	6		X		
PE-12	40	6			X	
PE-13	40	6	X			X
PE-14	40	6			X	X
PE-15 <sup>e</sup>	40	9		X		
PE-16 <sup>e</sup>	40	9		X		
PE-17 <sup>e</sup>	40	6		X		
PE-18 <sup>e</sup>	80	9		X		
PE-19	40	6		X		
PE-20	80	6		X		

<sup>a</sup>1 in. = 25.4 mm.

<sup>b</sup>PE stands for plastic collapse, elbow.

<sup>c</sup>See Fig. 3 for sign convention.

<sup>d</sup>A positive in-plane moment (+M<sub>z</sub>) causes the elbow to open; a negative in-plane moment (-M<sub>z</sub>) causes the elbow to close.

<sup>e</sup>Type 304L stainless steel elbow.

obtain the vertical and horizontal displacements at the weld at the loaded end of the elbow. With the additional information provided, the rotation  $\theta$  of the pipe extension in the plane of loading could be used in determining the collapse load. Forces were applied by hydraulic ram, and the magnitudes were measured using a strain-gage-based load cell.

Figure 4 is a photograph of specimen PE-16 under test.

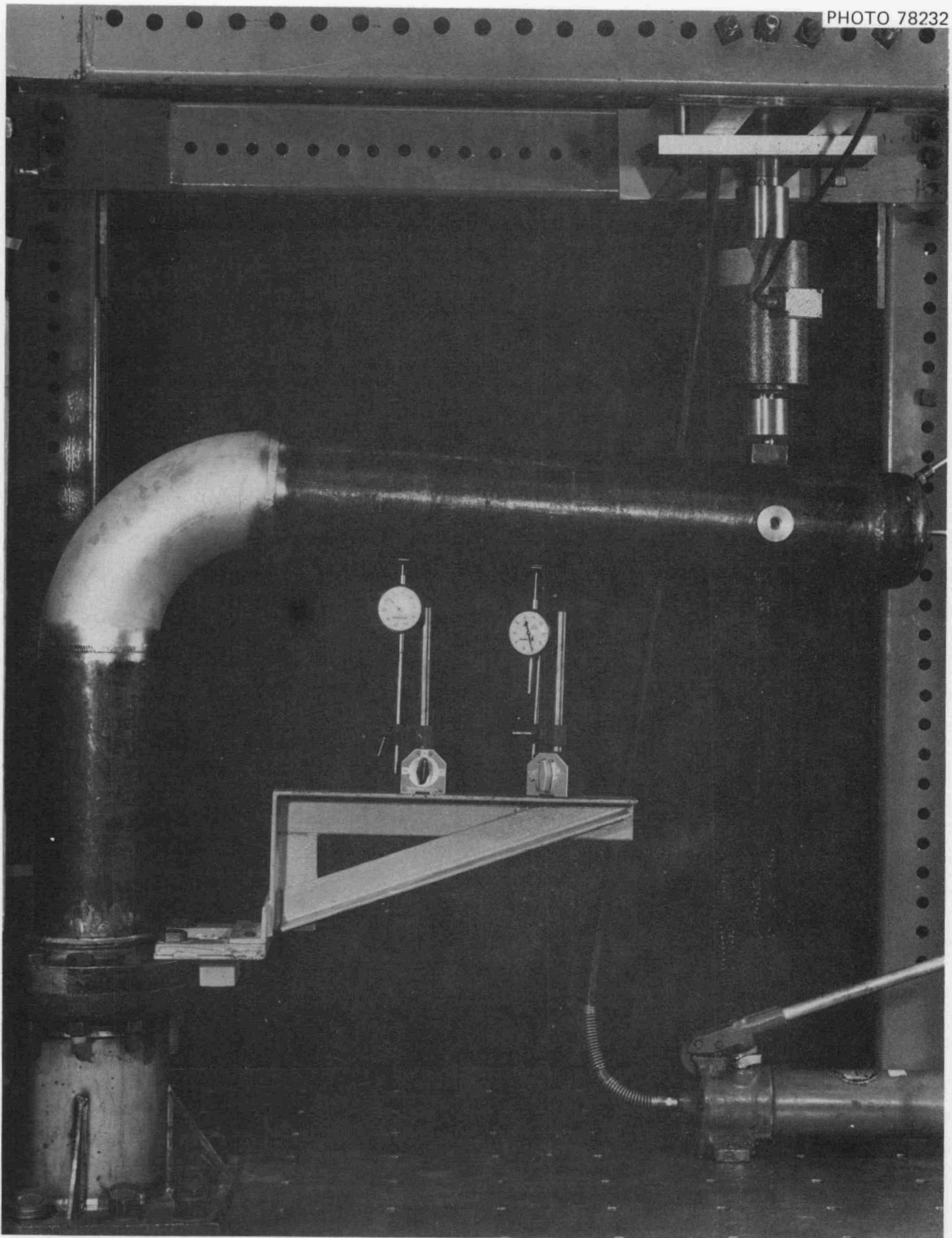


Fig. 4. Stainless steel elbow PE-16 during test.

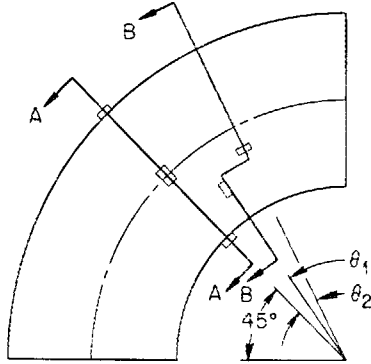
Strain gages were mounted on specimens PE-1, -2, -3, -8, -10, and -11 at the locations shown in Fig. 5. Single-element, bonded metallic-foil, electrical resistance strain gages with a 3.18-mm (1/8-in.) gage length were used in these tests. Ten three-gage strain rosettes with a delta configuration (Micromeasurements EA-06-030YB-120) were used for specimen PE-15; the gage length for the individual strain elements was 0.76 mm (0.030 in.). Their locations on the test assembly are shown in Fig. 6. Specimens PE-17, -18, -19, and -20 were more extensively instrumented than the others because gages were mounted on both the inside and the outside surfaces. The gage locations at the central cross section of these elbows are shown in Figs. 7 and 8.

Two types of gages were used at the locations shown in Figs. 7 and 8. Single three-gage rosettes with a 1.57-mm (0.062-in.) gage length (Micromeasurements EA-06-062RG-120) were designated type B and used for most locations. The second type of gage rosette, type A (Micromeasurements EA-06-030YB-120) was furnished by the manufacturer in stringers of five closely spaced units, with the rosettes spaced center to center at 3.18 mm (1/8 in.). (A stringer is shown in Fig. 9.) These stringers can be trimmed so that when two are fitted together, the spacing between end gages for the two stringers is 3.18 mm (1/8 in.).

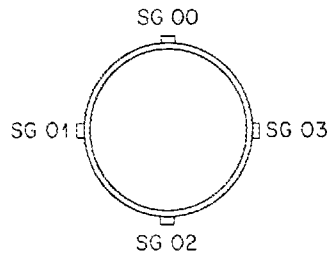
For reference, each type B rosette was designated according to its angular location; the type A rosettes were near the 90° location. The identification system used for each cross section is shown in Figs. 7 and 8. Type B rosettes were used on the outside at 90° for specimen PE-18 and on the inside at 90° for PE-20.

Brittle lacquer and birefringent coatings were also used on some specimens to verify that plastic collapse occurred in the elbows rather than in some other part of the system and to indicate locations and extents of plastic zones. The strain-gage data were used to examine details of behavior for elbows PE-17, -18, -19, and -20, but generally they were used to determine loads at which deviation from linear response occurred and to provide estimates of collapse loads. Quantitative analyses were not made with respect to the brittle lacquer and birefringent coatings.

ORNL-DWG 71-924R

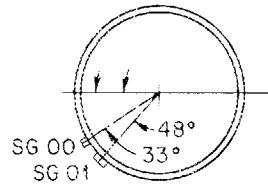


$\theta_1 = 4^\circ$   
 $\theta_2 = 9^\circ$



SECTION A-A

TEST PE-1 (FIG. 22)  
TEST PE-2 (FIG. 23)  
TEST PE-8 (FIG. 25)  
TEST PE-10  
TEST PE-11 (FIG. 26)



SECTION B-B

TEST PE-3 (FIG. 24)

Fig. 5. Diagram of strain-gage locations, PE-1, -2, -3, -8, -10, -11.

ORNL-DWG 77-20689

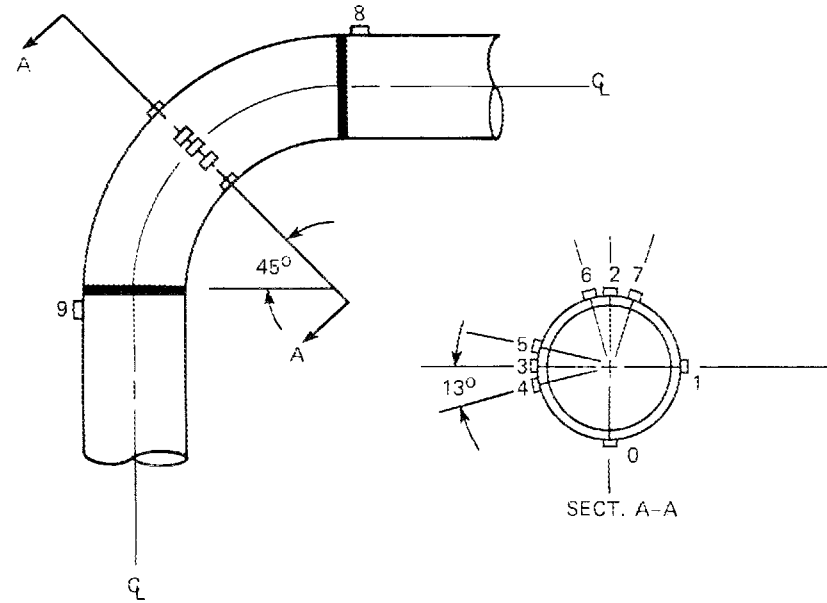


Fig. 6. Diagram of strain-gage locations, PE-15.

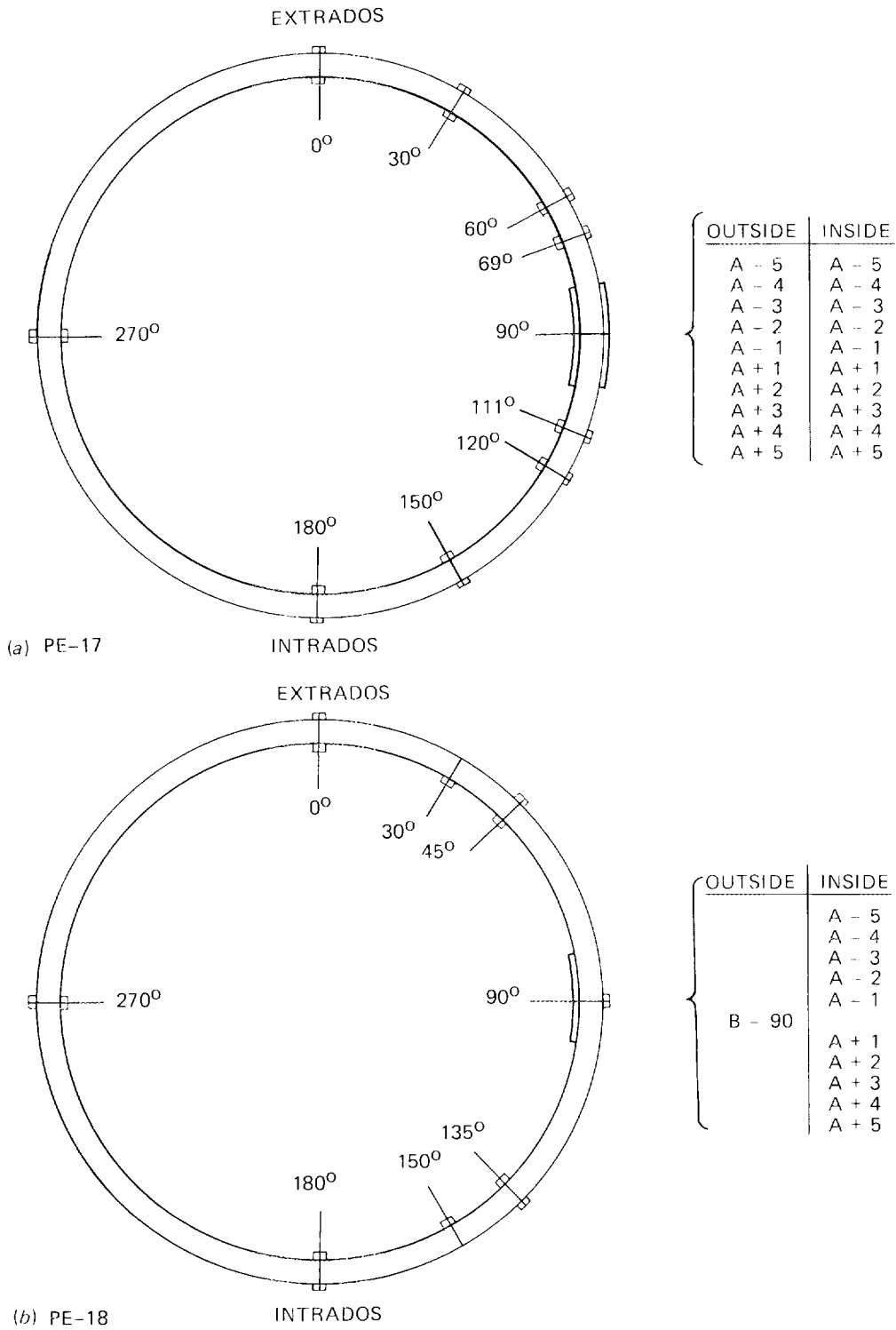


Fig. 7. Strain-gage locations on 45° cross-sectional planes of PE-18 and -19.

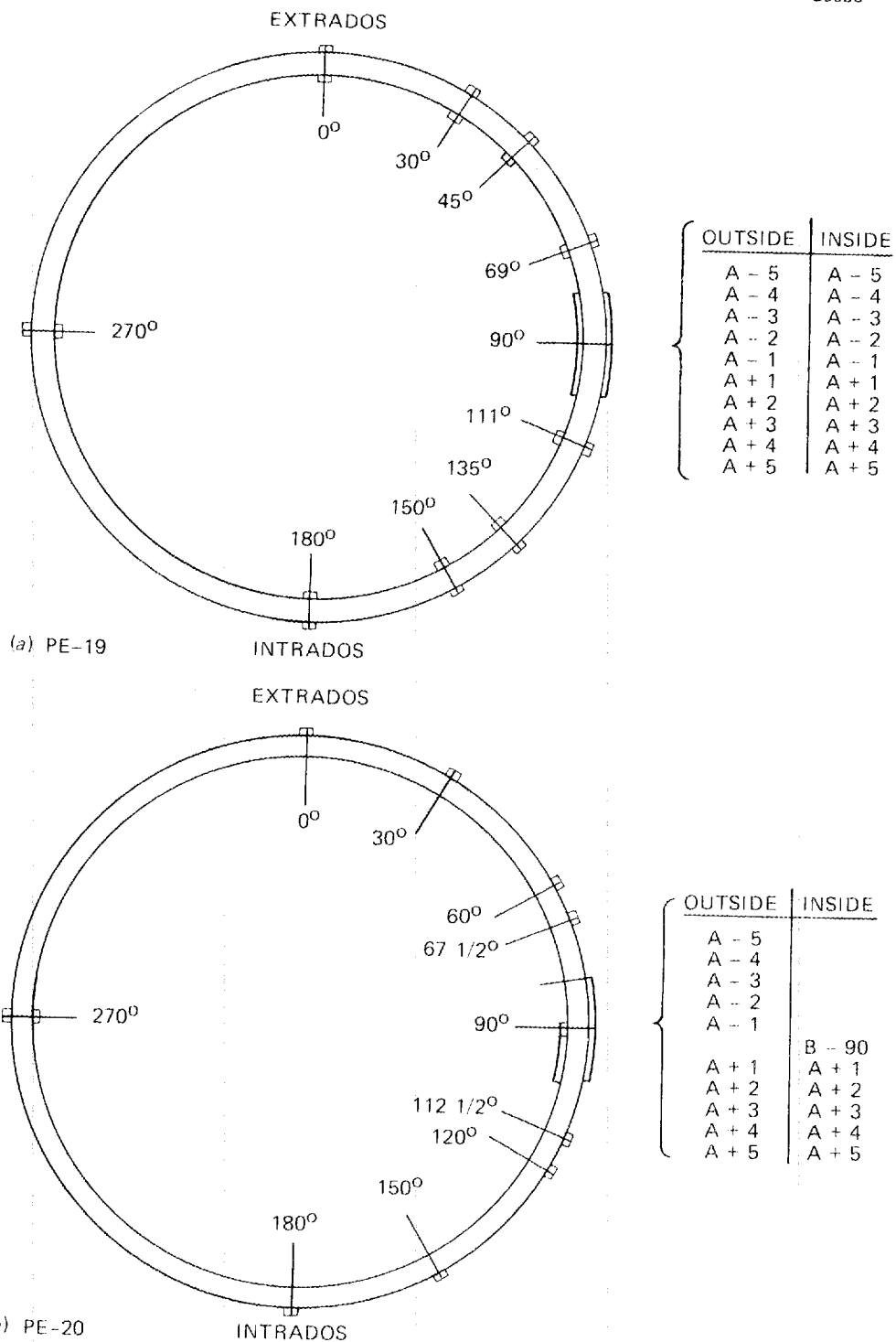


Fig. 8. Strain-gage locations on 45° cross-sectional planes of PE-19 and -20.

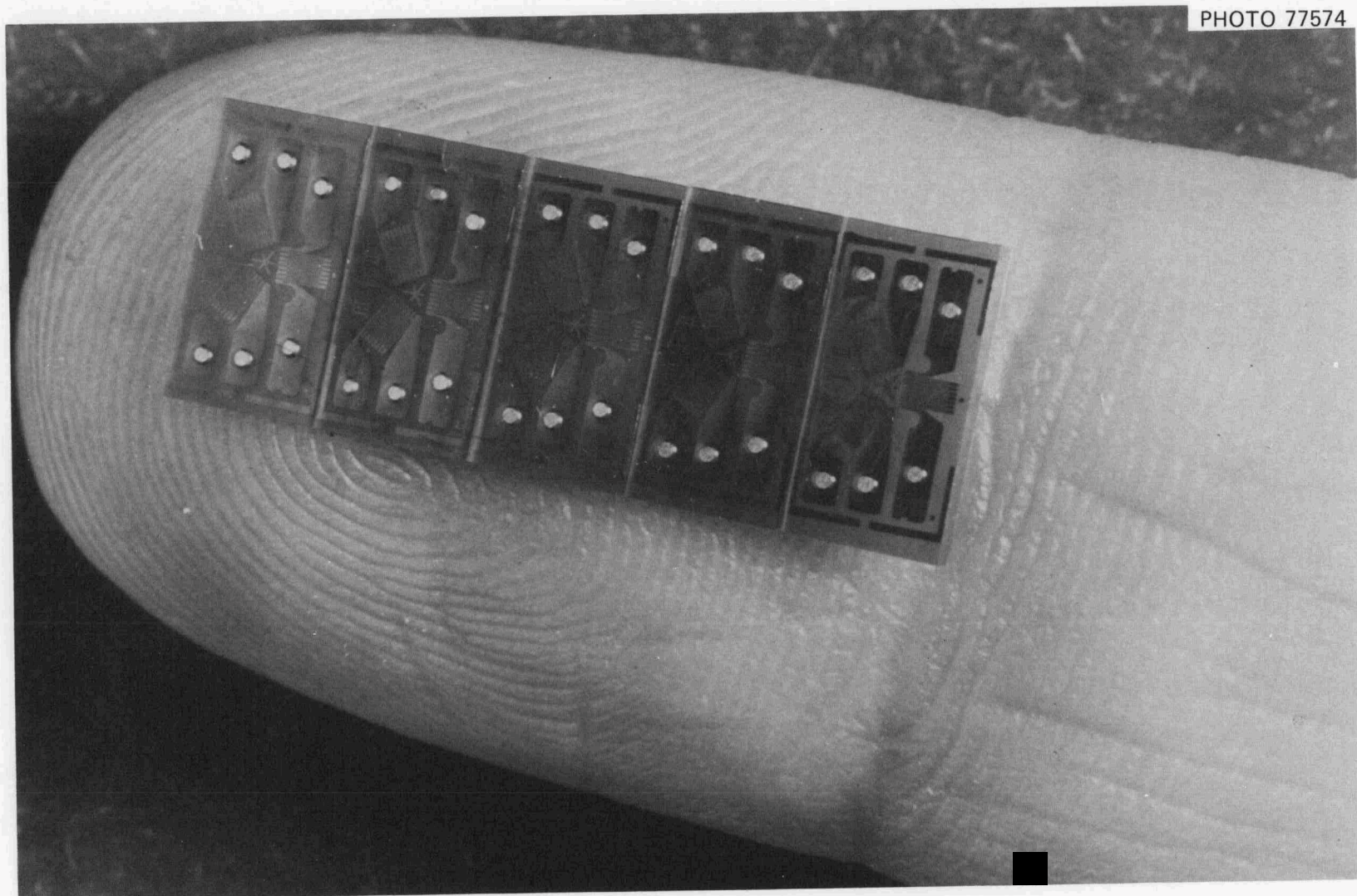


Fig. 9. Assembly of five strain-gage rosettes on common foil backing.

Each test was conducted by slowly applying the force loadings stepwise. The dial indicator readings were tabulated for each load increment, and the strain-gage data were recorded at each step with an automatic strain-gage scanning and indicating system, Binary Electronics model 205.

#### EXPERIMENTAL RESULTS

Load-deflection curves were obtained for all specimens; representative plots are included for illustration. Curves are shown for specimen PE-1 in Fig. 10, PE-2 in Fig. 11, and PE-3 in Fig. 12. These three specimens were long-radius, sched-40 elbows, and each was subjected to one of the three moment loadings employed (see Table 2). The curves show regions of initial linear (elastic) response and a gradual transition to predominantly plastic behavior.

In several instances, limitations on maximum loading ram travel and/or dial indicator travel limited the range of deflections that could be examined. However, in cases where the load-deflection curves extended well into the region of predominantly plastic behavior, there were no observable indications of alterations in response attributable either to geometry change effects or to strain hardening. One of the curves for PE-1 and one for PE-2 indicate these larger deflection trends.

Figures 13 and 14 show the load-deflection curves for specimens PE-8 (a sched-80 long-radius elbow) and PE-11 (a sched-40 short-radius elbow), respectively. The curves for PE-8 show leveling-off trends with increase in deflection.

The load-deflection curves for specimen PE-13 are shown in Fig. 15. In this case, the assembly was subjected to internal pressure plus force to produce an in-plane moment. Again, these curves show the initial elastic response and the gradual transition to predominantly plastic behavior. However, the slopes in the predominantly plastic region are much greater than those for the specimens discussed above and show stiffening which results from the addition of internal pressure.

Specimens PE-2, -15, and -16 were sched-40, long-radius elbows; the first was carbon steel and the others were stainless steel. Load-deflection curves for specimens PE-2 and -16 are plotted together in

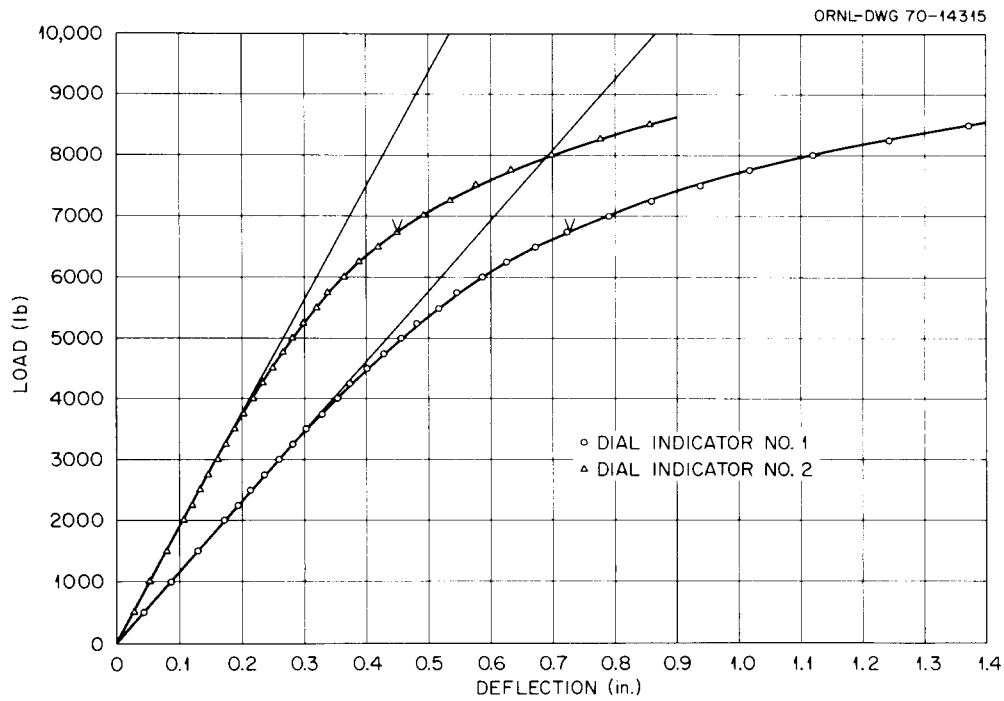


Fig. 10. Load-deflection curves for in-plane bending ( $+M_z$ ) of specimen PE-1 (1 in. = 25.4 mm; 1 lb<sub>f</sub> = 4.448 N).

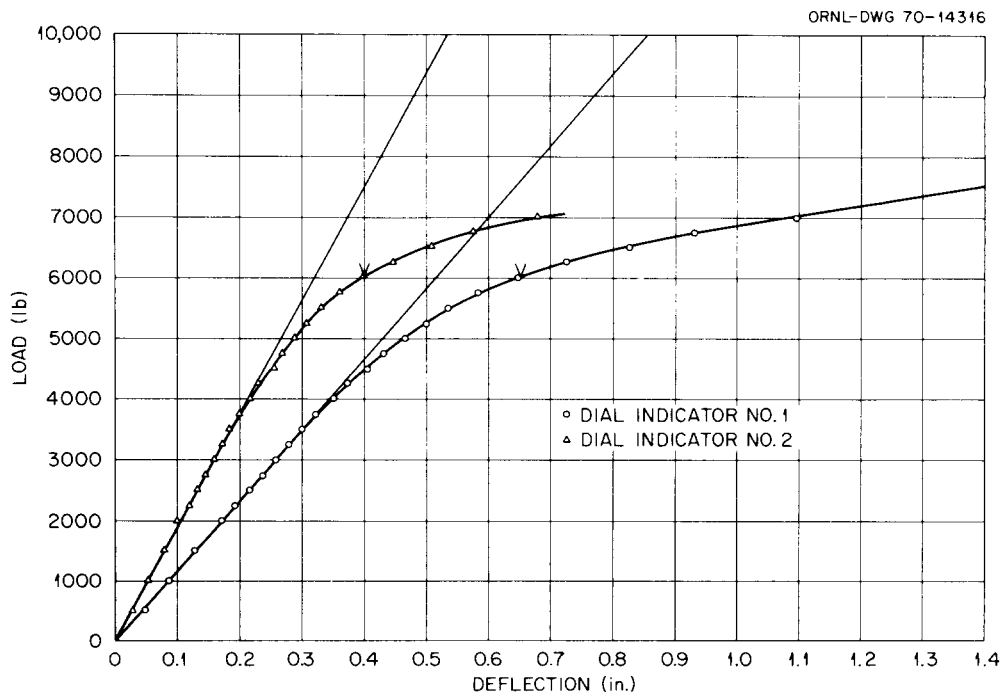


Fig. 11. Load-deflection curves for in-plane bending ( $-M_z$ ) of specimen PE-2 (1 in. = 25.4 mm; 1 lb<sub>f</sub> = 4.448 N).

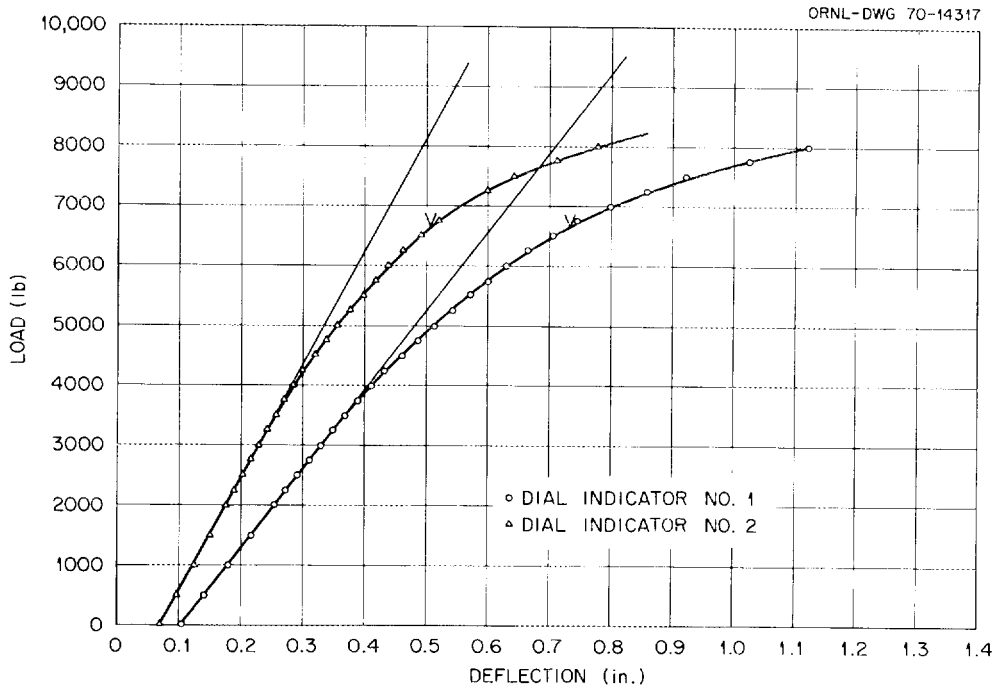


Fig. 12. Load-deflection curves for out-of-plane bending ( $M_y$ ) of specimen PE-3 (1 in. = 25.4 mm; 1 lb<sub>f</sub> = 4.448 N).

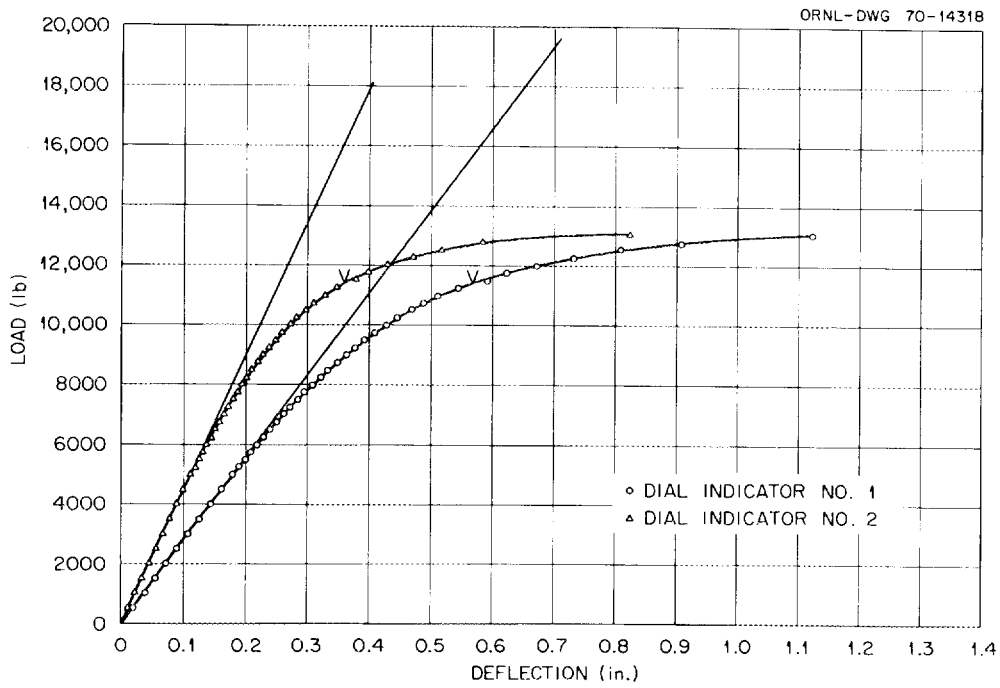


Fig. 13. Load-deflection curves for in-plane bending ( $-M_z$ ) of specimen PE-8 (1 in. = 25.4 mm; 1 lb<sub>f</sub> = 4.448 N).

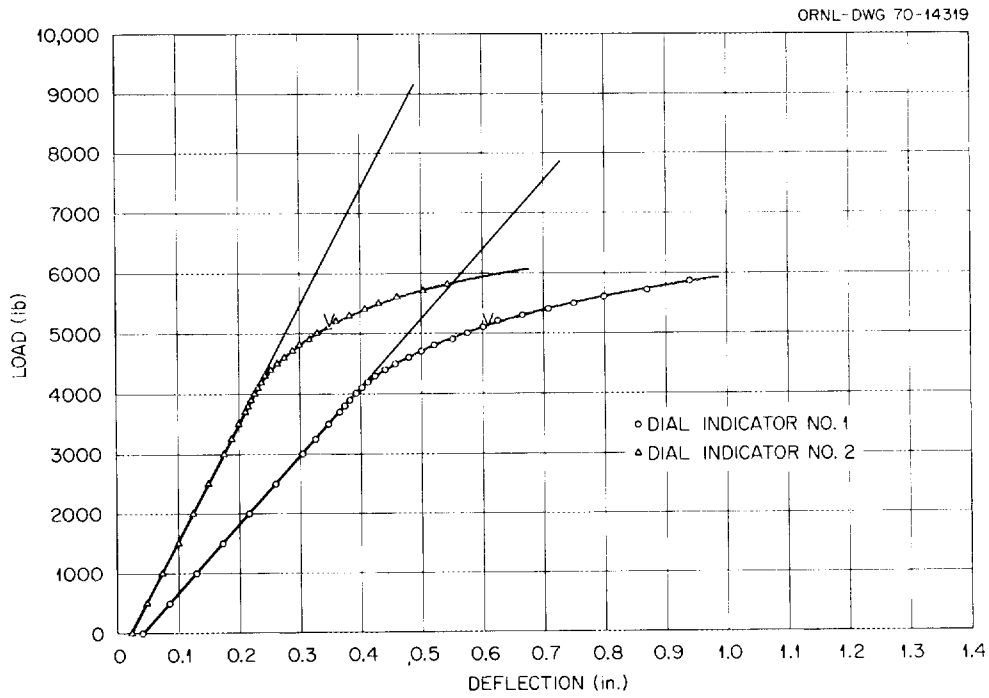


Fig. 14. Load-deflection curves for in-plane bending ( $-M_z$ ) of specimen PE-11 (1 in. = 25.4 mm; 1 lb<sub>f</sub> = 4.448 N).

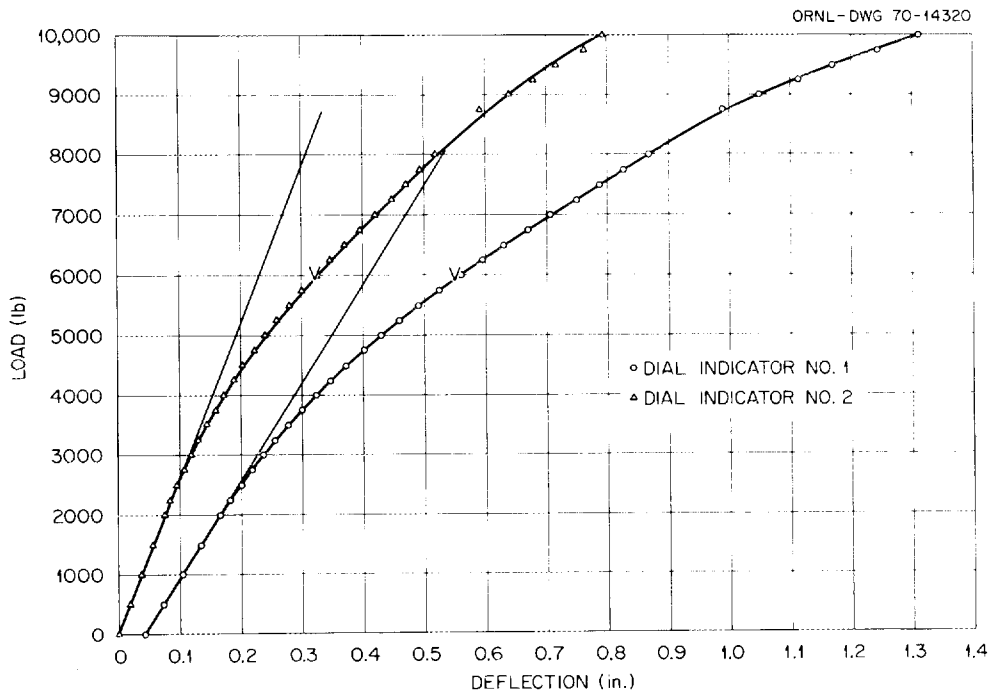


Fig. 15. Load-deflection curves for in-plane bending with internal pressure ( $M_z + P$ ) of specimen PE-13 (1 in. = 25.4 mm; 1 lb<sub>f</sub> = 4.448 N).

Fig. 16 to show differences in response for stainless steel and carbon steel specimens. The load-deflection curves for PE-15 (shown in Fig. 17) are very similar to those for PE-16. The collapse load for the carbon steel specimen is higher, but the transition from initial linear response to predominantly plastic response is more rapid than that for stainless steel.

Special care was given to the testing of PE-17 through -20. The test procedures were established to assure that the load-deflection curves would extend well into the region of predominantly plastic response; and, as noted, strain gages were mounted on both the inside and the outside of the elbows at the central cross section. These gages were for monitoring strain distributions as functions of load and for determining onset of nonlinear response from the individual load-strain histories. The load-deflection curves for each of the four specimens are given in Figs. 18 through 21.

The load-deflection curves of Figs. 18 through 21 show leveling off at the larger displacements, with the leveling-off trend being least pronounced for the sched-40 stainless steel elbow, PE-17. In Fig. 20, upper and lower load points are shown on the load-deflection plots for PE-19. The lower points were obtained for each displacement increment in the plastic range by holding the deflection fixed until the corresponding load decreased and stabilized.

Load-strain curves for specimens PE-1, -2, -3, -8, -11, and -15 are shown in Figs. 22 through 27. For the most part, the data selected were those for which the forces at 0.2% offset strain could be determined. The strain-gage numbers correspond to those in Figs. 5 and 6. The characteristics of these curves are similar to those of the corresponding load-deflection curves, with a small linear response portion for the stainless steel specimen. For the in-plane bending cases, the gages were located in planes in which the major and minor axes of ovality for the deformed cross section were expected to lie. In the case of out-of-plane bending, Fig. 24, the gages were mounted on the tension side of the elbow, again at locations near the position of the major axis of expected ovality. These gages were oriented as closely as possible with the directions of principal strains, as indicated by the brittle lacquer

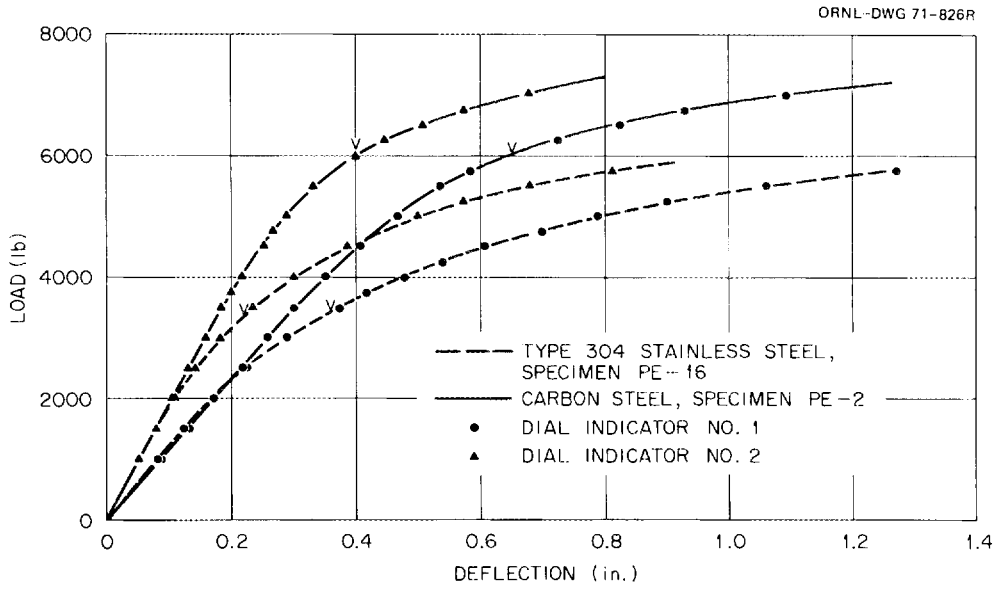


Fig. 16. Load-deflection curves for in-plane bending ( $-M_z$ ) of specimens PE-2 and PE-16 (1 in. = 25.4 mm; 1 lb<sub>f</sub> = 4.448 N).

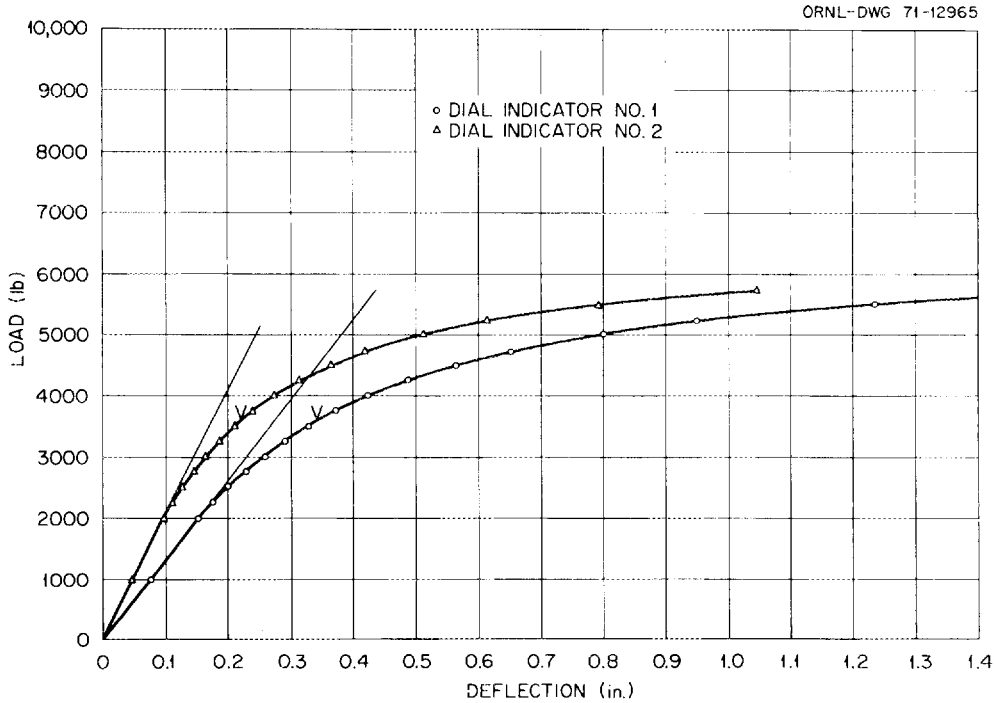


Fig. 17. Load-deflection curves for in-plane bending ( $-M_z$ ) of specimen PE-15 (1 in. = 25.4 mm; 1 lb<sub>f</sub> = 4.448 N).

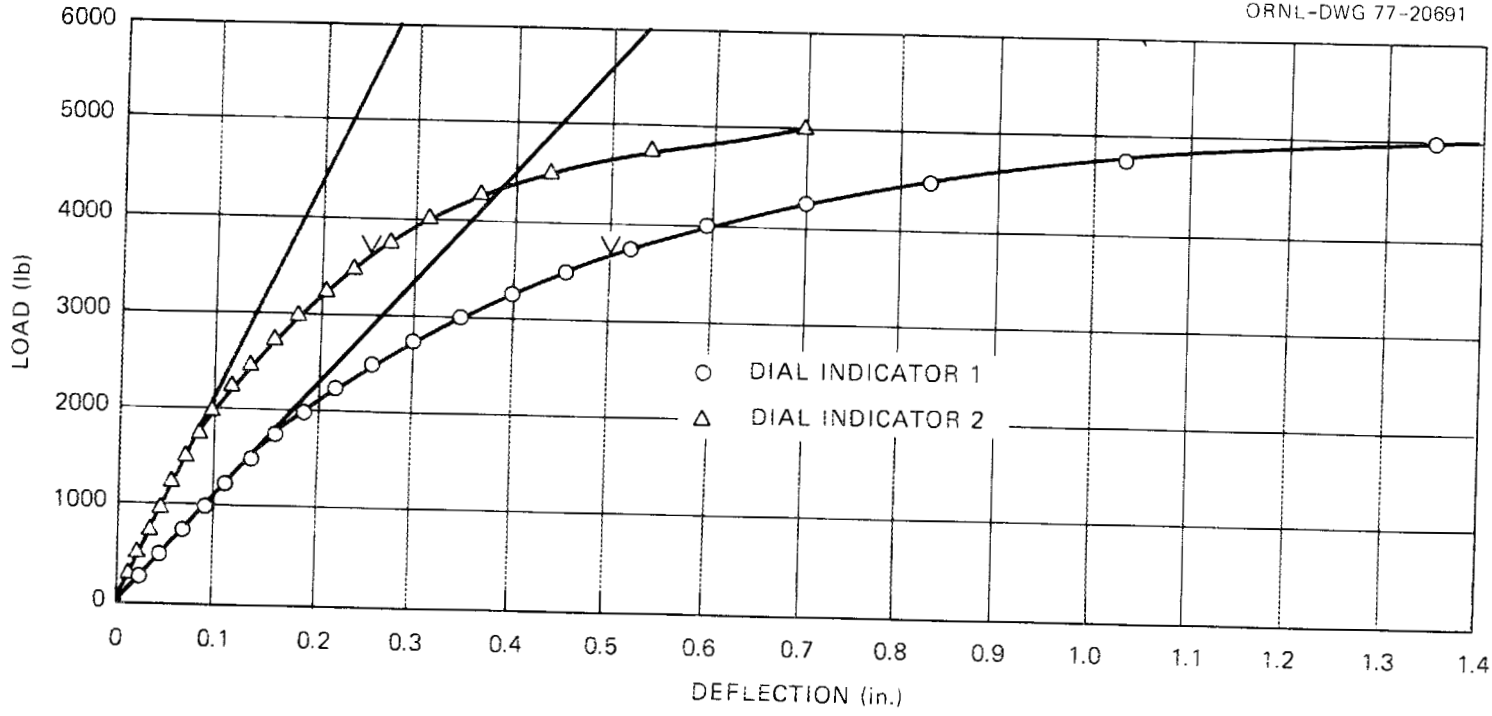


Fig. 18. Load-deflection curves for in-plane bending ( $-M_z$ ) of specimen PE-17 (1 in. = 25.4 mm; 1 lb<sub>f</sub> = 4.448 N).

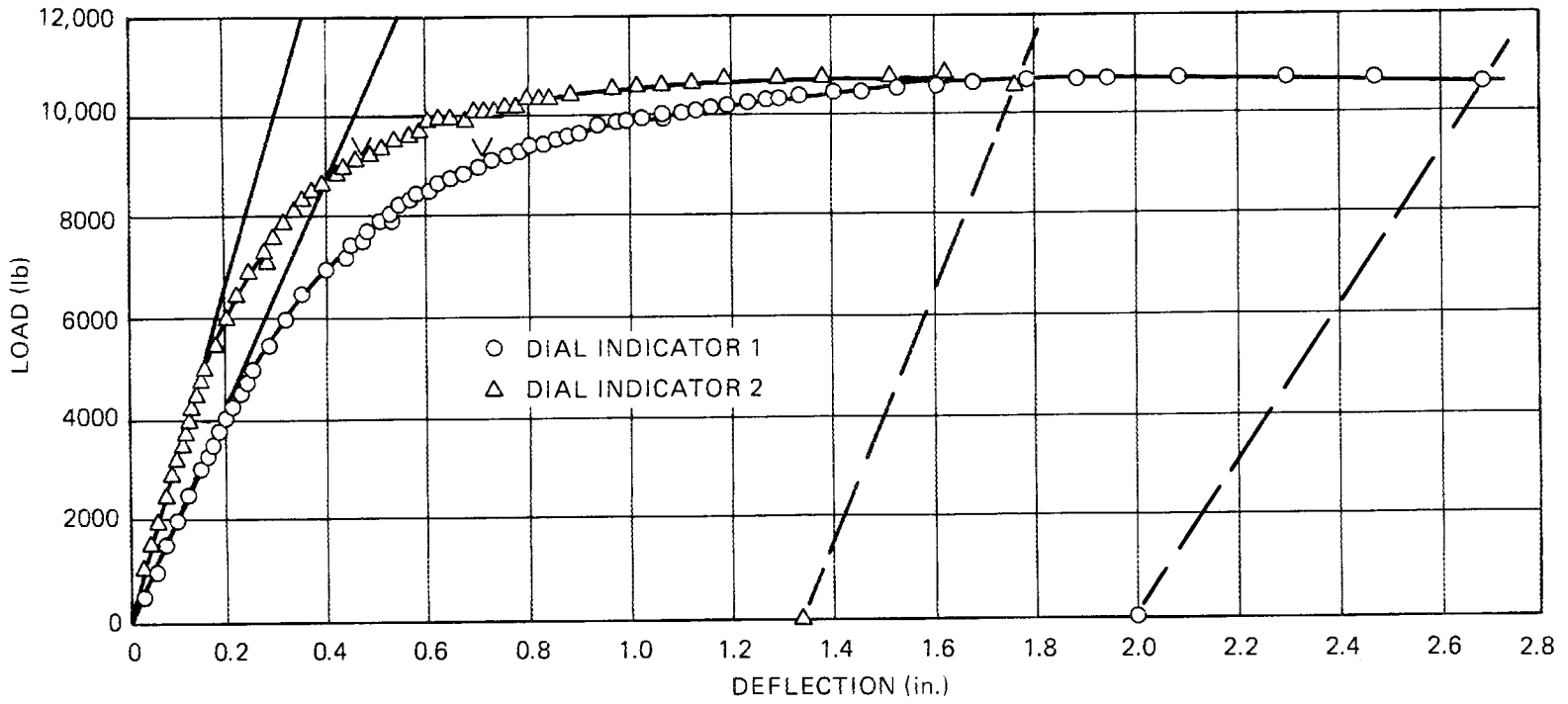


Fig. 19. Load-deflection curves for in-plane bending ( $-M_z$ ) of specimen PE-18 (1 in. = 25.4 mm; 1 lb<sub>f</sub> = 4.448 N).

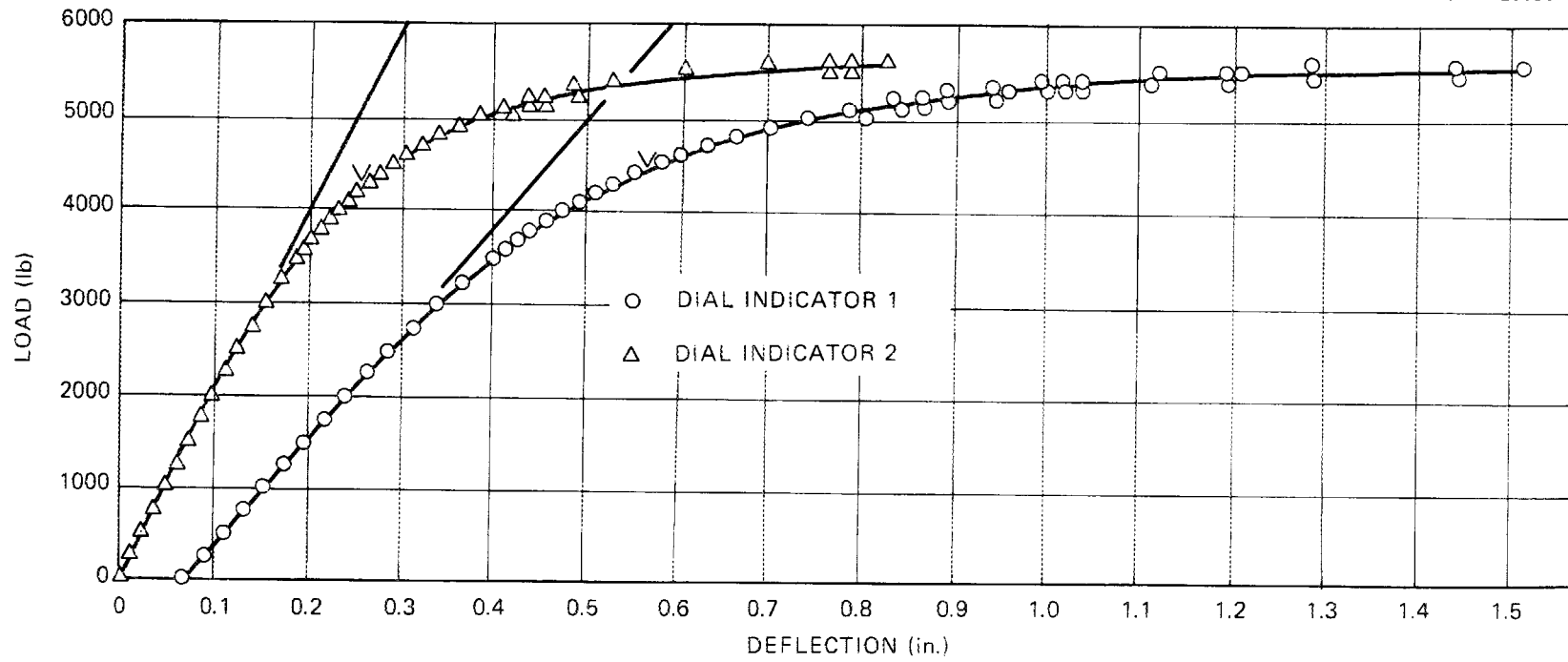


Fig. 20. Load-deflection curves for in-plane bending ( $-M_z$ ) of specimen PE-19 (1 in. = 25.4 mm; 1 lb<sub>f</sub> = 4.448 N).

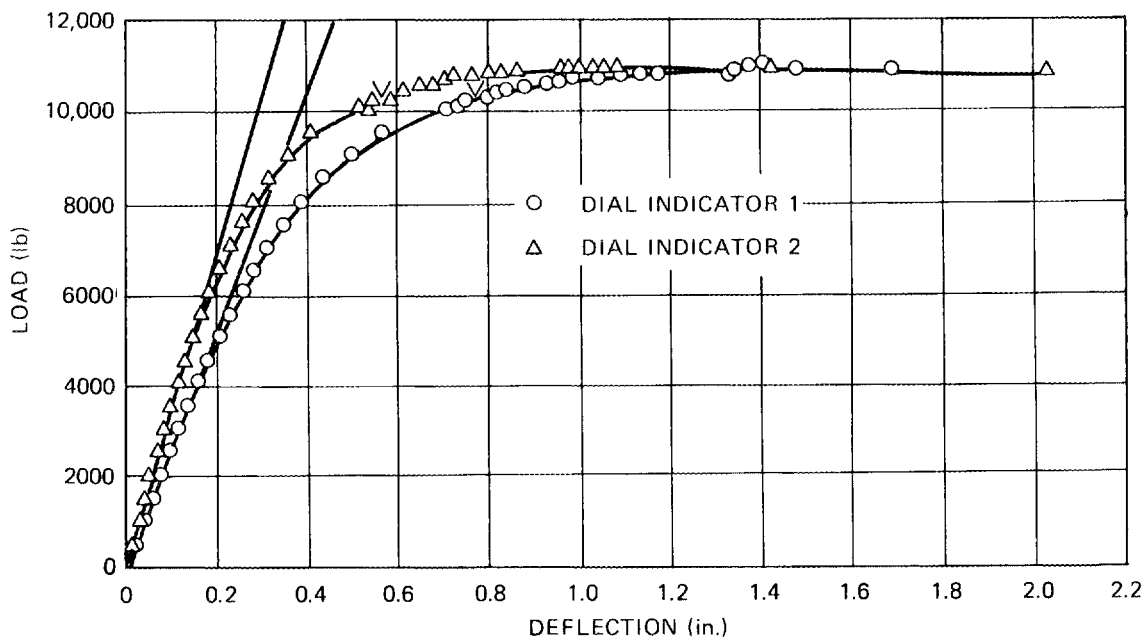


Fig. 21. Load-deflection curves for in-plane bending ( $-M_z$ ) of specimen PE-20 (1 in. = 25.4 mm; 1 lb<sub>f</sub> = 4.448 N).

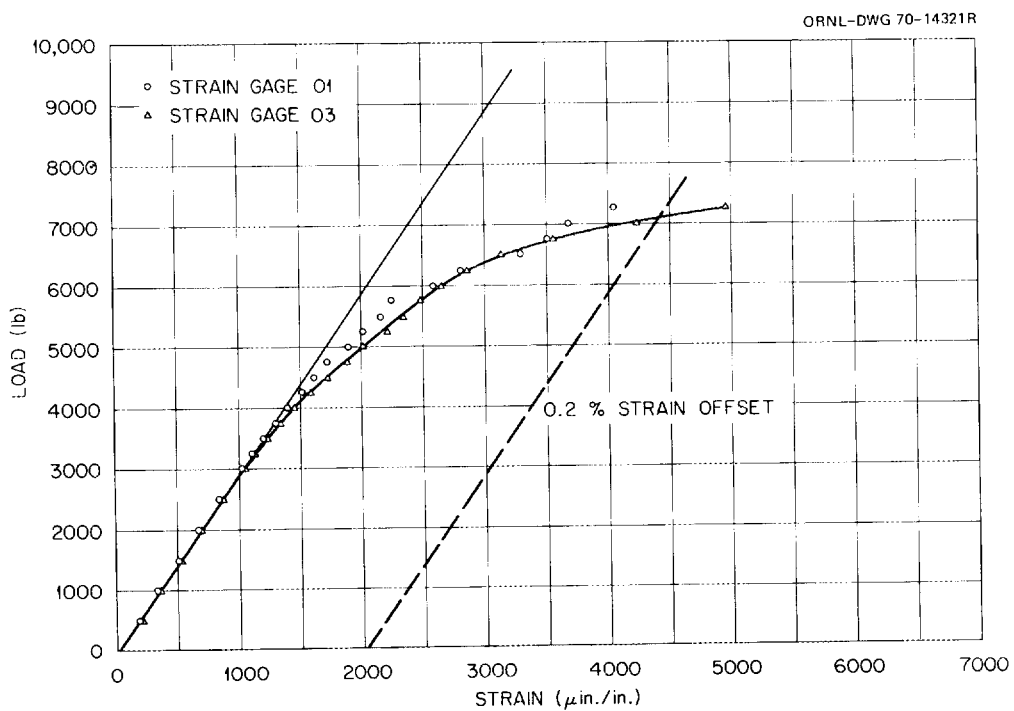


Fig. 22. Load-strain data for in-plane bending ( $+M_z$ ) of specimen PE-1 (1 lb<sub>f</sub> = 4.448 N).

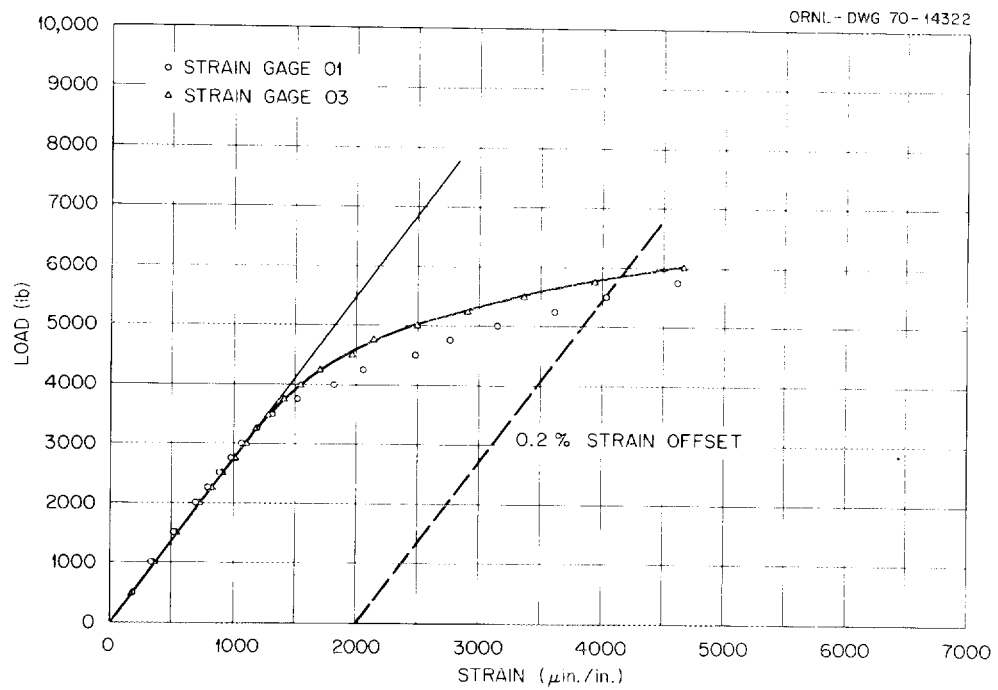


Fig. 23. Load-strain data for in-plane bending ( $-M_z$ ) of specimen PE-2 ( $1 \text{ lb}_f = 4.448 \text{ N}$ ).

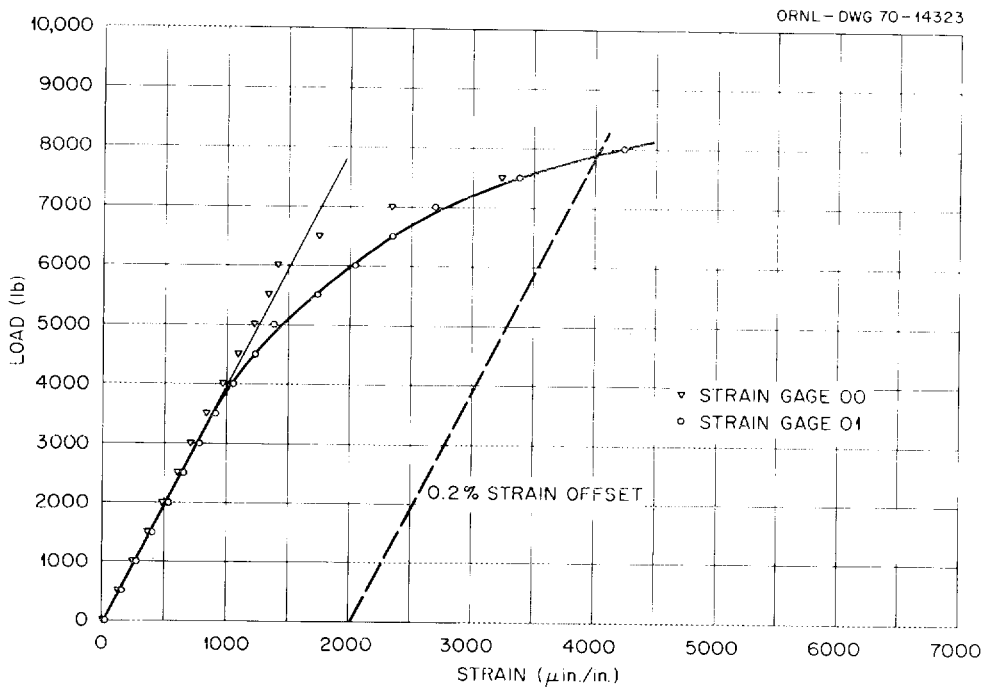


Fig. 24. Load-strain data for out-of-plane bending ( $M_y$ ) of specimen PE-3 ( $1 \text{ lb}_f = 4.448 \text{ N}$ ).

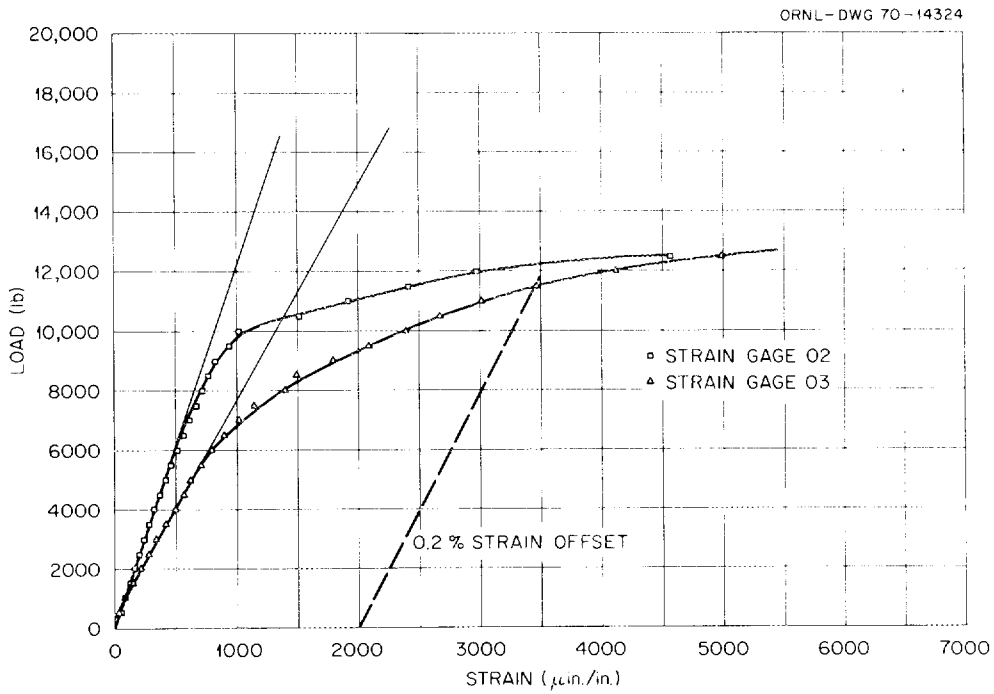


Fig. 25. Load-strain data for in-plane bending ( $-M_z$ ) of specimen PE-8 ( $1 \text{ lb}_f = 4.448 \text{ N}$ ).

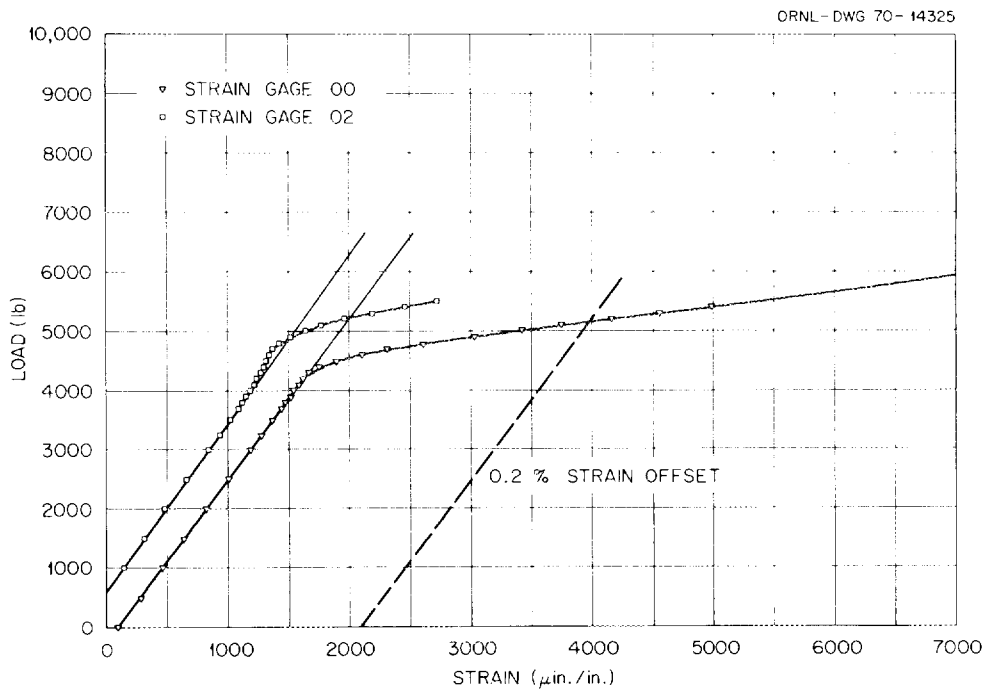


Fig. 26. Load-strain data for in-plane bending ( $-M_z$ ) of specimen PE-11 ( $1 \text{ lb}_f = 4.448 \text{ N}$ ).

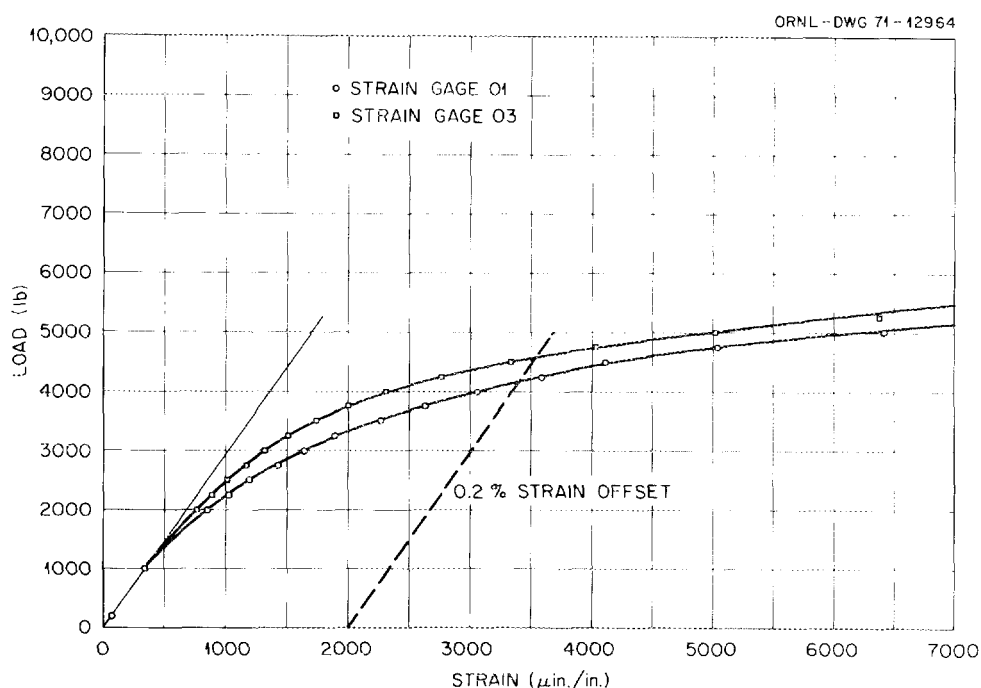


Fig. 27. Load-strain data for in-plane bending ( $-M_z$ ) of specimen PE-15 ( $1 \text{ lb}_f = 4.448 \text{ N}$ ).

tests. However, birefringent coating results indicated a significant difference between the location of maximum strain and the locations of the gages.

In the case of a negative in-plane moment ( $-M_z$ ), which tends to cause the bend radius of the elbow to decrease, the load-strain curves for carbon steel elbows show a relatively rapid transition from elastic to predominantly plastic behavior. For the curves shown in Fig. 26, the onset of nonlinear behavior, as indicated by strain gage 00 on the convex side (extrados) of the elbow, was accompanied by a tendency for an initial reduction in strain increase as a function of load on the concave side (intrados) of the elbow, as indicated by strain gage 02.

The load response of specimen PE-15 was also charted by plotting the angle of rotation,  $\theta$ , of the plane of the loaded end of the elbow (or, alternately, the rotation of the loaded extension) as a function of load. Values of  $\theta$  were calculated from the displacements measured at the end of the elbow and the deflections obtained from the two dial indicators

positioned as shown in Fig. 2. Load-vs-angle curves are shown in Fig. 28, where  $\theta_1$  and  $\theta_2$  were obtained from indicators DI 1 and DI 2, respectively.

Circumferential strain at the midplane ( $45^\circ$  plane) is plotted as a function of angular position in Figs. 29 and 30 for PE-18 and -19, respectively. The circumferential strain is the maximum principal strain, and the angular locations are as shown in Figs. 7 and 8. The curves shown are for constant loads as indicated on the curves for the inside surfaces. The load ranged from 15.57 to 44.26 kN (3500 to 9950 lb) for PE-18, and the range was from 6.67 to 22.24 kN (1500 to 5000 lb) for PE-19. These plots show that the maximum strain occurs on the inside surfaces near the  $90^\circ$  location.

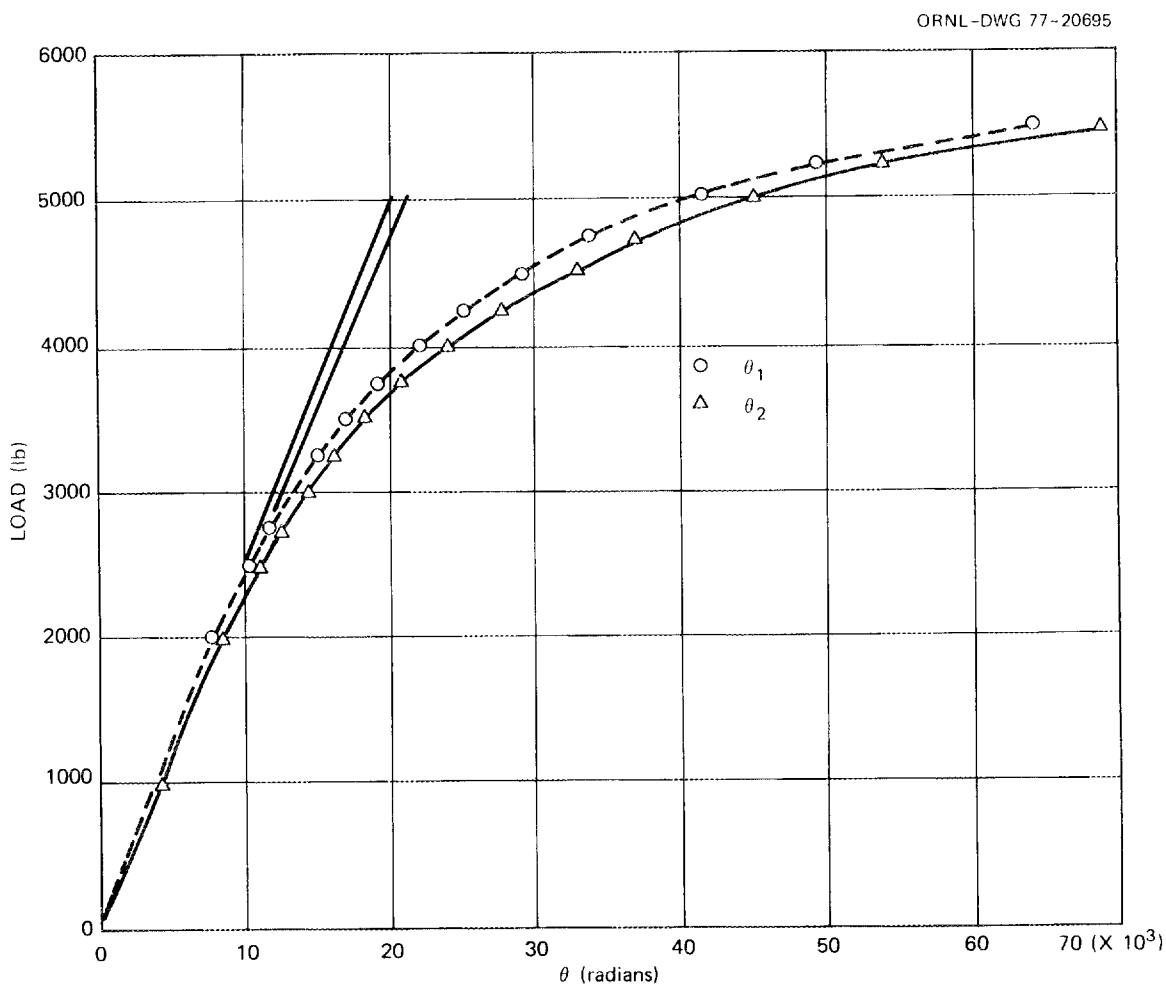


Fig. 28. Load-angle of rotation curves for in-plane bending ( $-M_z$ ) of specimen PE-15 ( $1 \text{ lb}_f = 4.448 \text{ N}$ ).

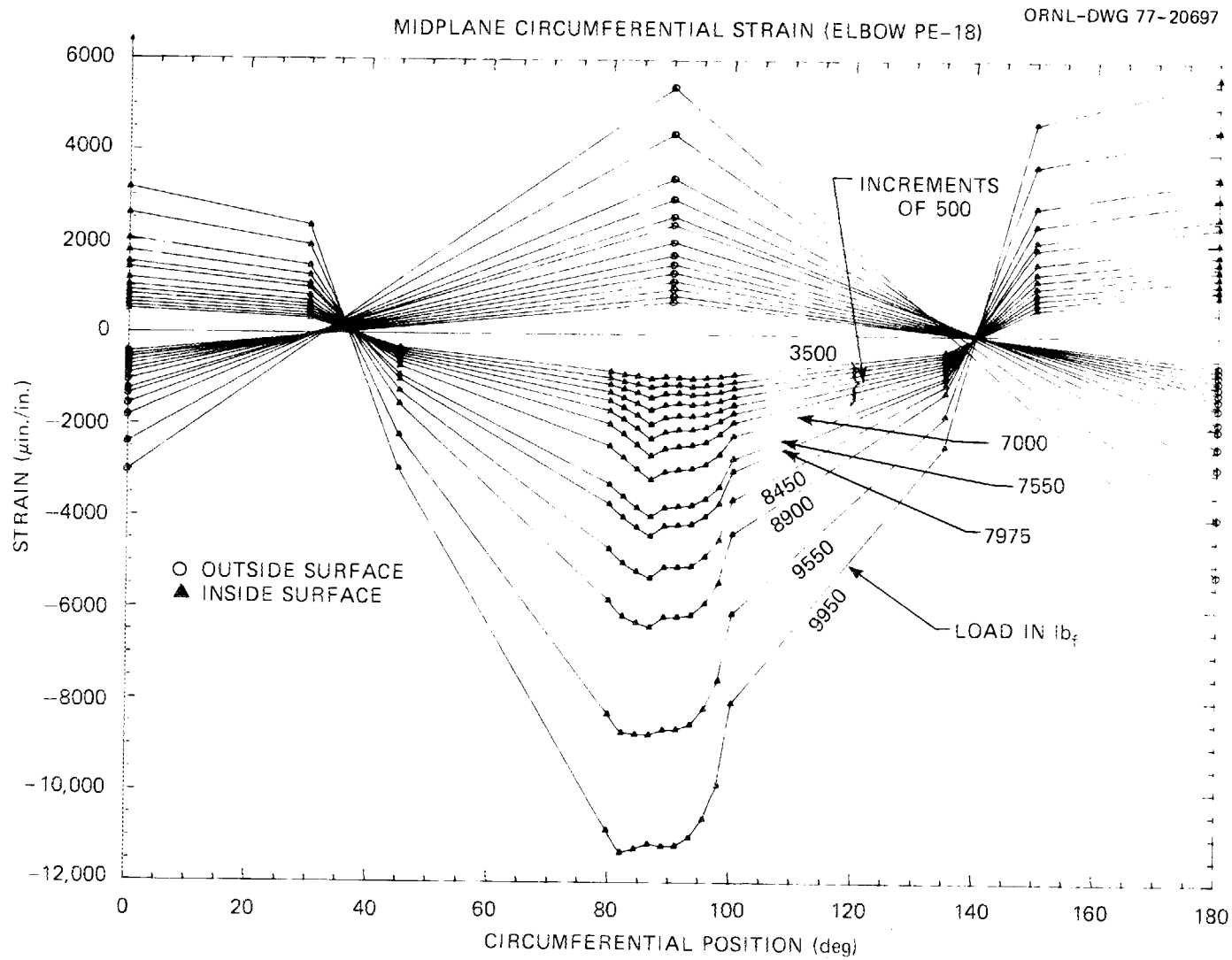


Fig. 29. Circumferential strain vs angular location as function of load for PE-18 ( $1 \text{ lb}_f = 4.448 \text{ N}$ ).

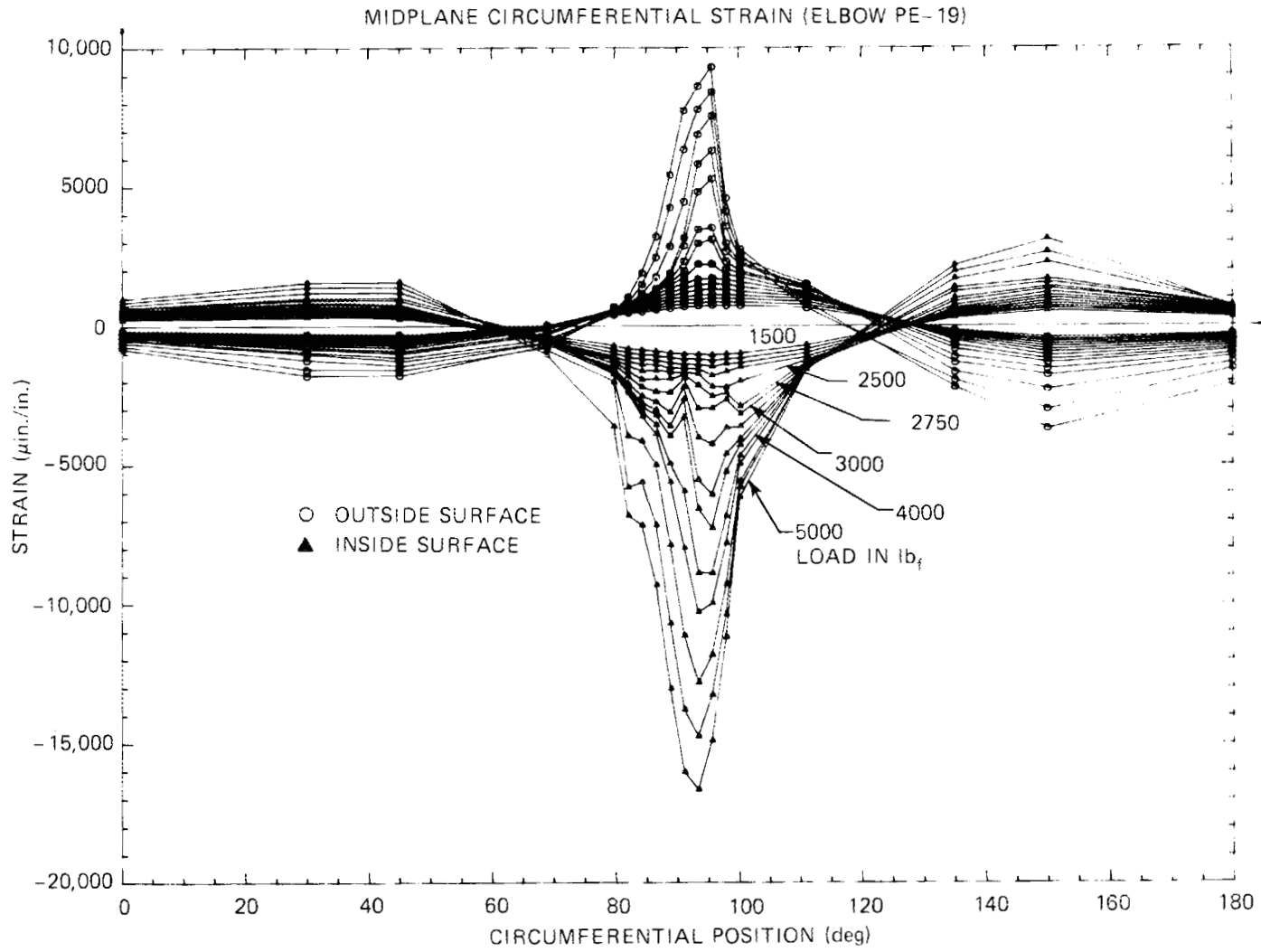


Fig. 30. Circumferential strain vs angular location as function of load for PE-19 ( $1 \text{ lb}_f = 4.448 \text{ N}$ ).

Load-strain curves for specimens PE-17 through -20 are given in Figs. 31 through 34. These curves are for gages mounted at or near the maximum strain point on the inside surface, except for PE-20 where data from a gage on the outer surface are plotted. The strain gage numbers correspond to those shown in Figs. 7 and 8.

Birefringent and brittle lacquer coatings were used on the tensile sides of two specimens which were subjected to out-of-plane loadings. In both cases, the region of maximum tensile stress was indicated to be

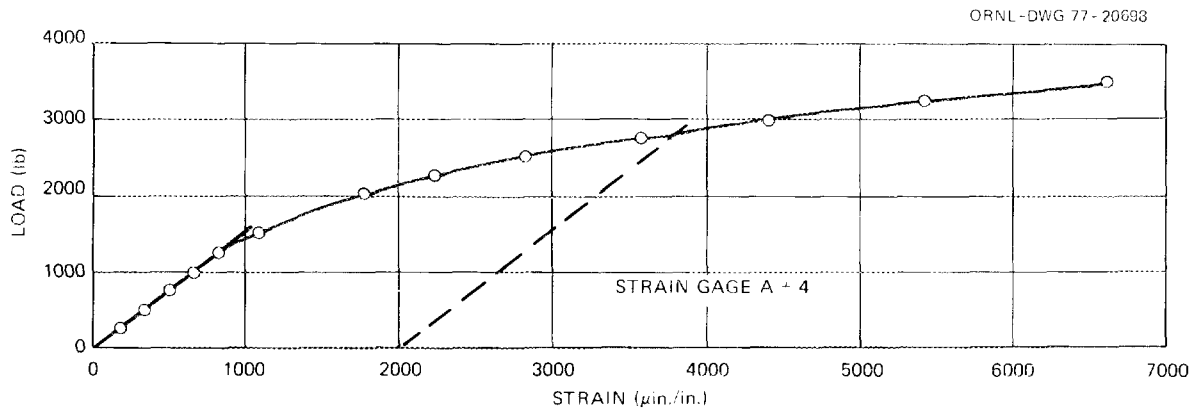


Fig. 31. Load-strain data for in-plane bending ( $-M_z$ ) of specimen PE-17 (1 in. = 25.4 mm; 1 lb<sub>f</sub> = 4.448 N).

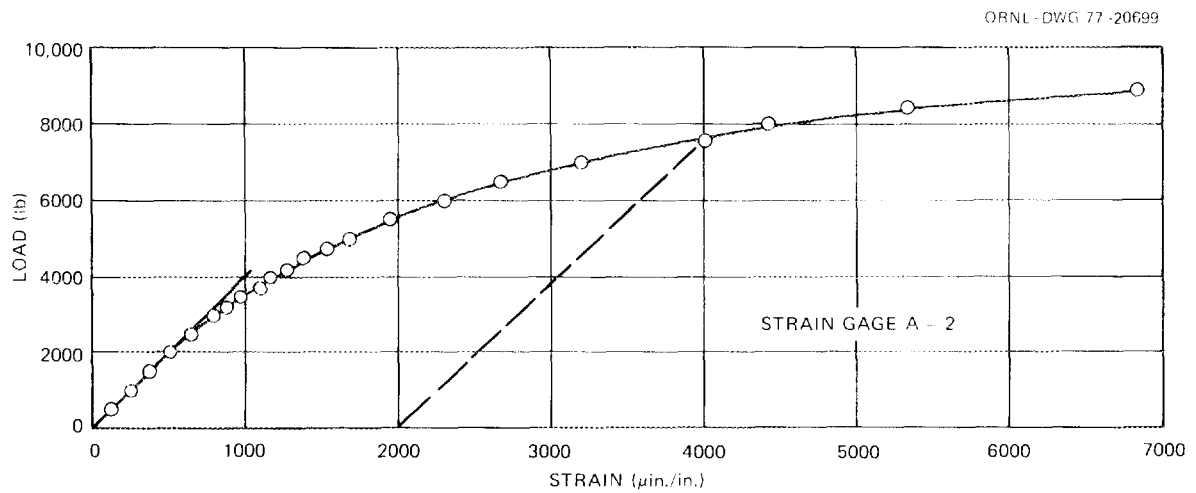


Fig. 32. Load-strain data for in-plane bending ( $-M_z$ ) of specimen PE-18 (1 in. = 25.4 mm; 1 lb<sub>f</sub> = 4.448 N).

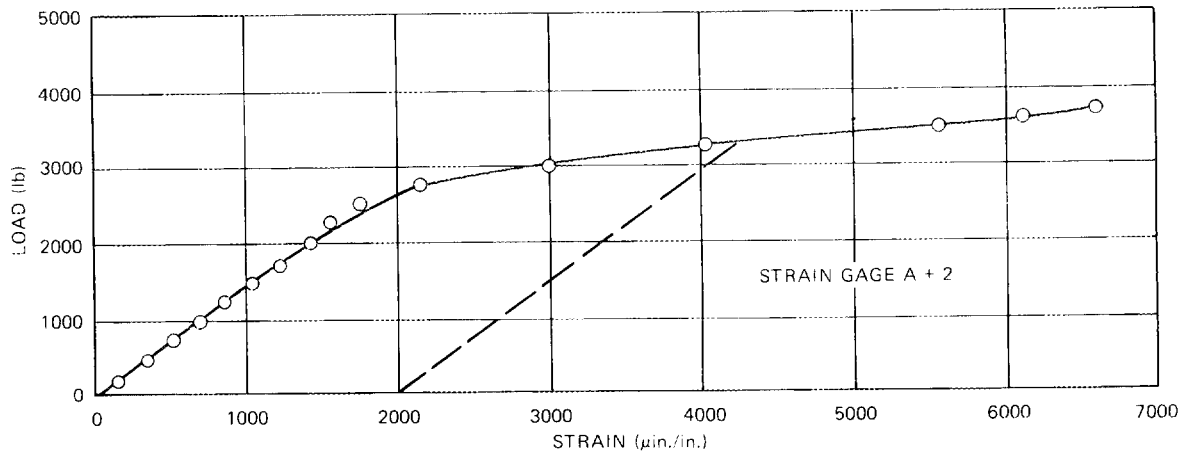


Fig. 33. Load-strain data for in-plane bending ( $-M_z$ ) of specimen PE-19 (1 in. = 25.4 mm; 1 lb<sub>f</sub> = 4.448 N).

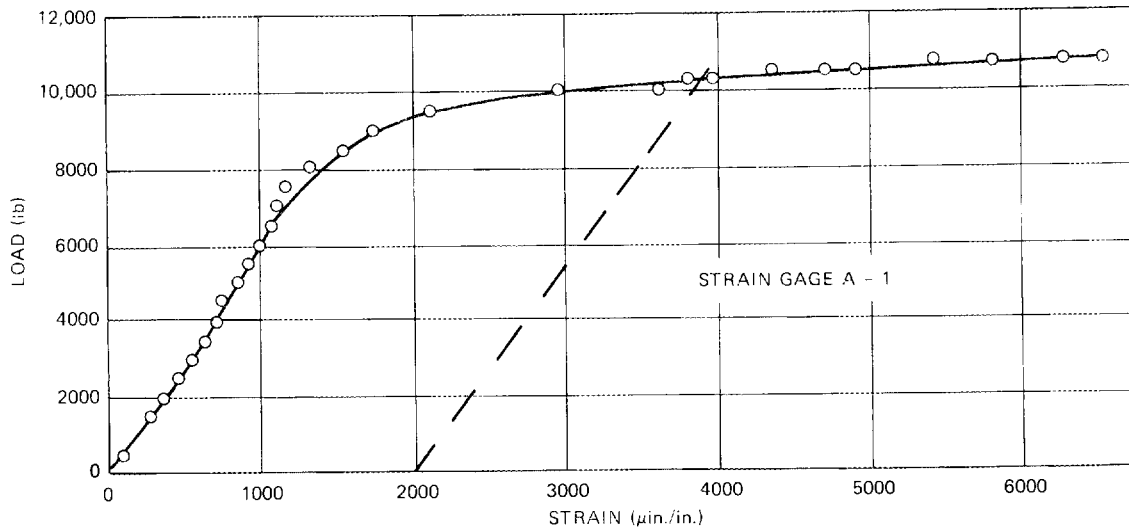


Fig. 34. Load-strain data for in-plane bending ( $-M_z$ ) of specimen PE-20 (1 in. = 25.4 mm; 1 lb<sub>f</sub> = 4.448 N).

essentially at the midplane or toward the concave side of the elbow. These observations are in line with results to be expected on the basis of elastic analyses.<sup>3</sup> The brittle lacquer coating revealed a region of maximum tensile stress approximately 38.1 mm (1 1/2 in.) wide and 304.8 mm (12 in.) in length along the surface at the midplane of PE-15, which was subjected to in-plane loading.

A dimensional survey<sup>4</sup> on selected commercial piping components was conducted at ORNL; this survey indicated that the maximum measured ovality for 101.6-mm (4-in.) sched-40 elbows was about 1.0%. The maximum ovality measured for the first 14 carbon steel specimens after test in this study was 6.5% for PE-1, which had been subjected to an in-plane bending moment. The stainless steel elbow, PE-15, had pretest ovalities of 1.0% at the ends and 2.0% at the 45° plane; after test, these ovalities were 5.3 and 10%, respectively. The posttest ovality at the 45° plane for the second stainless steel elbow, PE-16, was 9.4%.

Dimensional data for PE-17 through -20 were obtained before and after testing. These data included both diameters and thicknesses measured at the loaded and the fixed end and at the 45° plane of the elbow. (See the appendix.) All dimensions prior to test were within the limits given by applicable standards. Posttest ovalities are given in Table 3; the largest was 14.5% for PE-18, the sched-80 stainless steel elbow. The pretest ovalities were about 1% or less.

Table 3. Posttest ovalities

Specimen No.	Ovality (%)		
	Loaded end	45° plane	Fixed end
PE-17	4.7	9.3	5.4
PE-18	4.2	14.5	5.1
PE-19	5.6	7.6	5.9
PE-20	6.3	12.6	8.2

It is instructive to examine the extent of the region of initial linear (elastic) response for each specimen. The forces, or loads, corresponding to the point of departure from linear response are listed in Table 4. The strain-gage results are representative values obtained from the gages used, and the two values obtained from the dial indicators are listed for all specimens. There is reasonably good agreement

Table 4. Experimentally determined forces corresponding to departure from linear response

Test No.	Type of load	Type of elbow	Force (lb) at departure from linear response <sup>a</sup>		
			Strain gage	DI 1	DI 2
PE-1	+M <sub>z</sub>	Sched-40 LR	3250	3500	3500
PE-2	-M <sub>z</sub>	Sched-40 LR	3500	3750	3750
PE-3	M <sub>y</sub>	Sched-40 LR	3500	3750	3750
PE-4	+M <sub>z</sub> + P	Sched-40 LR		2500	2400
PE-5	-M <sub>z</sub> + P	Sched-40 LR		2800	3000
PE-6	M <sub>y</sub> + P	Sched-40 LR		3000	3000
PE-7	+M <sub>z</sub>	Sched-80 LR		7000	7500
PE-8	-M <sub>z</sub>	Sched-80 LR	5000	6000	5250
PE-9	M <sub>y</sub>	Sched-80 LR		5000	5000
PE-10	+M <sub>z</sub>	Sched-40 SR	3400	3200	3000
PE-11	-M <sub>z</sub>	Sched-40 SR	4050	4200	4100
PE-12	M <sub>y</sub>	Sched-40 SR		4000	3850
PE-13	+M <sub>z</sub> + P	Sched-40 SR		2500	2500
PE-14	M <sub>y</sub> + P	Sched-40 SR		2750	3000
PE-15	-M <sub>z</sub>	Sched-40 LR	1200	2200	2100
PE-16	-M <sub>z</sub>	Sched-40 LR		1900	1800
PE-17	-M <sub>z</sub>	Sched-40 SR	1150	1500	1500
PE-18	-M <sub>z</sub>	Sched-80 LR	2700	3000	3300
PE-19	-M <sub>z</sub>	Sched-40 SR	1400	2050	2150
PE-20	-M <sub>z</sub>	Sched-80 SR	3700	4000	4000

<sup>a</sup> 1 lb<sub>f</sub> = 4.448 N.

between the values for a given specimen in all cases except for the low strain-gage value for specimen PE-15.

The data in Table 4 for carbon steel elbows show that combinations of internal pressure and external force loading resulted in departures from linearity at loads which were lower than those for external forces

alone. A comparison of the values obtained from dial-indicator curves shows that the loads at the onset of nonlinear response for the stainless steel elbows are from 0.4 to 0.6 of those for corresponding carbon steel elbows subjected to the same loading conditions and with the same radii and wall thicknesses. These differences are not reflections of the differences in 0.2% offset yield stresses.

#### INTERPRETATION OF RESULTS

The determination of plastic collapse loads from tests on real structures for comparison with limit analysis calculations has been the subject of many discussions.<sup>1,5-10</sup> In general, a force-displacement curve for a structure displays a region of linear response, a transition region where the behavior changes from mainly elastic to mainly plastic, and a region in which a small increase in load produces a large change in displacement. The concept of plastic collapse for an ideal structure is the condition where deflections can increase without limit while the load is held constant. Thus, the selection of the collapse load for a real structure requires careful study.

Demir and Drucker,<sup>1</sup> in their studies on cylindrical specimens subjected to outwardly directed ring loadings, defined the limit load as the load at which the measured deflection was three times the extrapolated elastic deflection. The limit loads obtained in this way were in excellent agreement with theoretical predictions. According to the authors, the factor 3 was selected arbitrarily and represented a compromise between the larger and smaller factors which are sometimes used.

A second method for establishing the limit load is to use the point of intersection of a line drawn tangent to the initial portion of the force-deflection curve (the elastic response region) and a line drawn tangent to the straight-line portion of the curve in the plastic region. Of course this method depends upon the existence of a region in the predominantly plastic response range for which the deflection is directly proportional to the load, and thus the experiment must be carried beyond the transition region, and geometry change effects must be absent. A

third method is to determine the load at 0.2% offset strain from a load-strain diagram where the strains are measured by strain gages located in the high-stress or -strain regions of the structure.

The results corresponding to the intersecting line, or tangent, method described above are very close to those obtained using the total deflection criterion in the case of the experiments by Demir and Drucker. Thus, the two methods are essentially equivalent for their case. Other investigators<sup>6,7,11</sup> have shown that the tangent method gives results which compare favorably with calculated limit-load values for other shell structures and loadings. In addition, reasonable agreement has also been found between the load at 0.2% offset strain and the load obtained using the tangent method.<sup>7,9,10</sup>

The results from the series of tests on 152.4-mm (6-in.) elbows indicated continuous decreases in deformation resistance with increase in load. However, as mentioned in the preceding section, there were cases in which limitations on maximum loading ram travel and/or dial indicator travel precluded obtaining curves which extended far enough into the plastic region to show linear response at the higher loads. In addition, strain-gage results were obtained only for a few cases. Thus a method patterned after that used by Demir and Drucker was established for obtaining limit-load values on the basis of total deflection. The means for selecting the deflection values is described below.

Results for those specimens where collapse loads could be obtained by the 0.2% offset strain method, by the tangent method, or by both are given in Table 5. Values were determined by the tangent method for both load-deflection curves for PE-14, -15, -18, -19, and -20. A comparison of the results obtained by the two methods for specimens PE-1, -2, -11, and -20 shows very good agreement between strain gage (0.2% offset) and dial-indicator (tangent) data. There is also close agreement between the strain-gage result for PE-15 and the dial indicator values. The strain gage results are low for PE-17, -18, and -19. It is noted that the loads which were determined from the load-strain and the load-deflection curves (Table 4) and which correspond to the onset of nonlinear response were generally found to be in good agreement for all but one specimen, PE-15, where there was a significant difference between these values.

Table 5. Experimentally determined loads using selected criteria

Test No.	Type of load	Type of elbow	Collapse load <sup>a</sup> (lb)		
			0.2% offset strain	Tangent method	
				DI 1	DI 2
PE-1	+M <sub>z</sub>	Sched-40 LR	7,100		6,875
PE-2	-M <sub>z</sub>	Sched-40 LR	5,700		6,175
PE-3	M <sub>y</sub>	Sched-40 LR	7,900		
PE-5	-M <sub>z</sub> + P	Sched-40 LR		7,925	
PE-6	M <sub>y</sub> + P	Sched 40 LR		7,250	
PE-7	+M <sub>z</sub>	Sched-80 LR		13,750	
PE-8	-M <sub>z</sub>	Sched-80 LR	11,900		
PE-9	M <sub>y</sub>	Sched-80 LR		12,900	
PE-11	-M <sub>z</sub>	Sched-40 SR	5,150		5,150
PE-13	+M <sub>z</sub> + P	Sched-40 SR		6,800	
PE-14	M <sub>y</sub> + P	Sched-40 SR		6,200	6,750
PE-15	-M <sub>z</sub>	Sched-40 LR	4,400	4,160	4,160
PE-16	-M <sub>z</sub>	Sched-40 LR		4,475	
PE-17	-M <sub>z</sub>	Sched-40 SR	2,850	3,700	
PE-18	-M <sub>z</sub>	Sched-80 LR	7,600	9,100	9,100
PE-19	-M <sub>z</sub>	Sched-40 SR	3,300	4,750	5,000
PE-20	-M <sub>z</sub>	Sched-80 SR	10,700	10,220	10,300

$$^a 1 \text{ lb}_f = 4.448 \text{ N.}$$

It is important to note that stress-strain curves for carbon steel in the strain range of interest in this report are close to those corresponding to the elastic, perfectly plastic behavior assumed in the development of limit analysis theory. But stainless steel, which shows a gradual transition from elastic to elastic-plastic behavior, exhibits response characteristics that are significantly different from the idealized behavior assumed. For this reason, it is justifiable to

establish the method of limit-load determination based on the response data for the carbon steel specimens only.

Since the loads for 0.2% offset strain and those determined from load-deflection curves through the use of the tangent method have been shown by others to give good comparisons with calculated limit loads, the agreement found between results obtained by these methods for the carbon steel specimens in this series of tests suggests that the tangent or an equivalent method can properly be used here for limit-load definition. In order to establish an equivalent method, the extrapolated elastic deflection,  $\delta E$ , was subtracted from the total deflection corresponding to the limit load in each case where the tangent method could be used. The difference, or the nonelastic deflection (denoted by  $a\delta E$ ), was divided by the elastic deflection to determine "a" and representative a values were selected. (Note that Demir and Drucker used  $a = 2$ .) These selected values, listed in Table 6, were then used to determine the collapse loads for each specimen. The collapse loads determined in this way are those associated with the "V" marks on the curves in Figs. 10 through 21. The collapse moments,  $M^*$ , at the ends of the elbows are the product, to the nearest 113.0 N·m (1000 in.-lb), of the collapse loads and the moment arms; these moments are also given in Table 6.

The collapse load for PE-3, as indicated in Table 6, is significantly less than the load determined by the 0.2% offset strain method (Table 5). This is also true for the collapse loads listed in Tables 5 and 6 for specimen PE-15. The magnitude of this difference for PE-15 is about the same as that for PE-3. The difference for PE-3 may be attributable to failure to locate the strain gages in the high strain region, as noted in the preceding section. However, this is not the contributing factor in the case of the stainless steel elbow, PE-15. The collapse loads for this specimen determined by the tangent method from the load vs  $\theta_1$  and the load vs  $\theta_2$  curves (Fig. 28) are the same, 18.5 kN (4160 lb). The corresponding values obtained from these load-vs- $\theta$  curves using the displacement method adopted for this study are 15.57 kN (3500 lb) and 15.79 kN (3550 lb). Thus, the first set of values for PE-15 are in reasonable agreement with the 0.2% offset strain value (Table 5), while the latter values agree with those given in Table 6 which were obtained from the load-deflection curves.

Table 6. Summary of data from limit load studies of 6-in. elbows<sup>a</sup>

Test No.	Wall schedule	Type of elbow	Material	Type of loading	a	Collapse load (lb)			Moment arm (in.)	Collapse moment, M* (in.-lb)	$\sigma = M^*/Z$ (psi)	Yield stress, $\sigma_0$ (psi)	$\frac{(M^*/Z)}{\sigma_0}$
						DI 1	DI 2	Average					
PE-1	40	LR	ASTM A-106B	+M <sub>z</sub>	0.25	6,750	6,750	6,750	28 1/2	192,000	22,800	50,000	0.46
PE-2	40	LR	ASTM A-106B	-M <sub>z</sub>	0.25	6,000	6,000	6,000	28 1/4	170,000	20,000	50,000	0.40
PE-3	40	LR	ASTM A-106B	M <sub>y</sub>	0.25	6,700	6,650	6,675	28 3/4	192,000	22,700	50,000	0.46
PE-4	40	LR	ASTM A-106B	+M <sub>z</sub> + P	0.40	7,500	7,200	7,350	27 9/16	203,000	24,000	50,000	0.48
PE-5	40	LR	ASTM A-106B	-M <sub>z</sub> + P	0.40	7,950	7,800	7,875	27 1/2	217,000	25,700	50,000	0.51
PE-6	40	LR	ASTM A-106B	M <sub>y</sub> + P	0.40	7,450	7,700	7,575	27 3/4	210,000	24,900	50,000	0.50
PE-7	80	LR	ASTM A-106B	+M <sub>z</sub>	0.40	13,850	13,900	13,875	25	347,000	28,500	37,800	0.75
PE-8	80	LR	ASTM A-106B	-M <sub>z</sub>	0.40	11,525	11,300	11,412	25	285,000	23,500	37,800	0.62
PE-9	80	LR	ASTM A-106B	M <sub>y</sub>	0.40	12,700	12,800	12,750	25 7/8	330,000	27,100	37,800	0.72
PE-10	40	SR	ASTM A-106B	+M <sub>z</sub>	0.25	5,525	5,300	5,413	29 3/4	161,000	19,100	39,600	0.48
PE-11	40	SR	ASTM A-106B	-M <sub>z</sub>	0.25	5,100	5,150	5,125	30	154,000	18,200	39,600	0.46
PE-12	40	SR	ASTM A-106B	M <sub>y</sub>	0.25	6,100	6,000	6,050	28	169,000	20,100	39,600	0.51
PE-13	40	SR	ASTM A-106B	+M <sub>z</sub> + P	0.40	5,950	5,950	5,950	27 1/2	164,000	19,400	39,600	0.49
PE-14	40	SR	ASTM A-106B	M <sub>y</sub> + P	0.40	6,100	6,250	6,175	27	167,000	19,800	39,600	0.50
PE-15	40	LR	ASTM A-312 (304L)	-M <sub>z</sub>	0.25	3,600	3,600	3,600	26 3/4	96,000	11,300	37,700	0.30
PE-16	40	LR	ASTM A-312 (304L)	-M <sub>z</sub>	0.25	3,500	3,400	3,450	27 1/2	95,000	11,200	37,700	0.30
PE-17	40	SR	ASTM A-312 (304L)	-M <sub>z</sub>	0.50	3,700	3,650	3,675	30	110,000	12,900	35,600	0.36
PE-18	80	LR	ASTM A-312 (304L)	-M <sub>z</sub>	0.70	9,100	9,200	9,150	27	247,000	20,200	35,400	0.57
PE-19	40	SR	ASTM A-106B	-M <sub>z</sub>	0.25	4,500	4,250	4,375	30	131,000	15,400	46,000	0.34
PE-20	80	SR	ASTM A-106B	-M <sub>z</sub>	1.0	10,220	10,300	10,260	30	307,800	25,188	34,600	0.73

<sup>a</sup>1 in. = 25.4 mm; 1 lb<sub>f</sub> = 4.448 N; 1 in.-lb = 1.1298 × 10<sup>-1</sup> N·m; 1 psi = 6.895 × 10<sup>3</sup> Pa.

Further, since essentially the same results are obtained from load-vs-deflection curves as from load-vs-angle of rotation curves, the selection of correlating parameters has little influence in this case.

The maximum bending stresses in the pipe extensions (the stresses,  $\sigma = M^*/Z$ , corresponding to the collapse moments,  $M^*$ ) were also calculated and listed in Table 6. The symbol  $Z$  denotes the section modulus for the pipe extension, or the elbow.

Because of the differences in yield stresses for the elbows (Table 1), comparisons must be made on the basis of the values in the last column of Table 6. These values, which range from 0.34 to 0.75 for carbon steel (0.30 to 0.57 for stainless steel), can be interpreted as indicating the margins of safety with respect to the onset of yield in straight runs of pipe.

The results given in Table 6 show that the ratio of the maximum bending stresses at collapse to the yield stresses are generally slightly larger for the short-radius sched-40 carbon steel elbows than for the sched-40 long-radius elbows for a given loading. In general, the addition of internal pressure increases the collapse moment, although the load at the onset of nonlinear response is decreased as noted in the preceding section. The ratio of maximum stress at collapse to yield stress is increased with increased wall thickness, and the collapse moments for stainless steel tend to be much smaller than those for carbon steel.

To give additional perspective, loads corresponding to first yield ( $L_{0.2\%}$ ), the proportional limit ( $L_{PL}$ ), the onset of nonlinear response as determined from strain gage readings ( $L_{SG}$ ),\* and the onset of nonlinear response as determined from dial gages ( $L_{DI}$ ), were considered. These are listed in Table 7 along with the bend characteristic parameter  $\lambda$  as given by

$$\lambda_1 = \frac{tR}{r^2\sqrt{1-\nu^2}},$$

---

\* Note that only specimens with inside gages were considered, except for PE-15.

Table 7. Summary of loads<sup>a</sup>

Test No.	Type of loading	$\lambda_1$	$\lambda_2$	R/r	$\psi$	Load at onset of yield <sup>b</sup> (lb)		Load at onset of nonlinearity <sup>c</sup> (lb)		Limit load <sup>c</sup> (lb)
						L <sub>0.2%</sub>	L <sub>PL</sub>	L <sub>SG</sub>	L <sub>DI</sub>	
PE-1	+M <sub>z</sub>	0.262	0.250	2.84	0	2814		3500		6,750
PE-2	-M <sub>z</sub>	0.262	0.250	2.84	0	2838		3750		6,000
PE-3	M <sub>y</sub>	0.262	0.250	2.84	0	3414		3750		6,675
PE-4	+M <sub>z</sub> + P	0.262	0.250	2.84	0.0045	2193		2450		7,350
PE-5	-M <sub>z</sub> + P	0.262	0.250	2.84	0.0045	2198		2900		7,875
PE-6	M <sub>y</sub> + P	0.262	0.250	2.84	0.0045	2681		3000		7,575
PE-7	+M <sub>z</sub>	0.425	0.405	2.91	0	4866		7250		13,875
PE-8	-M <sub>z</sub>	0.425	0.405	2.91	0	4866		5625		11,412
PE-9	M <sub>y</sub>	0.425	0.405	2.91	0	5619		5000		12,750
PE-10	+M <sub>z</sub>	0.175	0.167	1.89	0	1558		3100		5,413
PE-11	-M <sub>z</sub>	0.175	0.167	1.89	0	1545		4150		5,125
PE-12	M <sub>y</sub>	0.175	0.167	1.89	0	2073		3925		6,050
PE-13	+M <sub>z</sub> + P	0.175	0.167	1.89	0.0019	1065		2500		5,950
PE-14	M <sub>y</sub> + P	0.175	0.167	1.89	0.0019	1363		2875		6,175
PE-15	-M <sub>z</sub>	0.262	0.250	2.84	0	2260	809	1200	2150	3,600
PE-16	-M <sub>z</sub>	0.262	0.250	2.84	0	2198	787		1850	3,450
PE-17	-M <sub>z</sub>	0.175	0.167	1.89	0	1389	624	1150	1500	3,675
PE-18	-M <sub>z</sub>	0.425	0.405	2.91	0	4216	2144	2700	3150	9,150
PE-19	-M <sub>z</sub>	0.175	0.167	1.89	0	1795		1500	2100	4,375
PE-20	-M <sub>z</sub>	0.284	0.270	1.94	0	2710		3700	4000	10,260

<sup>a</sup>L<sub>0.2%</sub> = load at 0.2% offset strain; L<sub>PL</sub> = load at proportional limit; L<sub>SG</sub> = load at onset of nonlinearity as determined by strain gage results; L<sub>DI</sub> = load at onset of nonlinearity as determined by dial indicator results.

<sup>b</sup>Assumes yielding is determined by maximum shear stress; 1 lb<sub>f</sub> = 4.448 N.

<sup>c</sup>1 lb<sub>f</sub> = 4.448 N.

or

$$\lambda_2 = \frac{tR}{r^2}.$$

Also given in Table 7 are the radius ratio R/r, and the pressure parameter,

$$\psi = \frac{PR^2}{ERt}.$$

In these equations, t is the thickness of the elbow, r is the mean radius, R is the bend radius,  $\nu$  is Poisson's ratio, E is the elastic

modulus, and P is pressure. The last column of Table 7 gives the limit loads. The loads corresponding to onset of yielding were calculated using stress indices derived from Ref. 12 and assuming that yield is determined by the maximum shear stress. The  $L_{PL}$  values for the stainless steel specimens are low compared with those for  $L_{SG}$ . For PE-19 and -20, the  $L_{0.2\%}$  and  $L_{SG}$  values are in fair agreement.

Moments corresponding to the loads given in Table 7 were normalized using  $M^*$ , the plastic collapse moment in each case, and the resultant values are listed in Table 8. The last column of this table gives the ratio of the plastic collapse moment to the theoretical plastic collapse

Table 8. Summary of moment ratios

Test No.	Type of loading	$\lambda_2$	R/r	Onset of yield		Onset of nonlinearity		Straight pipe normalization
				$\frac{M_{0.2\%}}{M^*}$	$\frac{M_{PL}}{M^*}$	$\frac{M_{SG}}{M^*}$	$\frac{M_{DI}}{M^*}$	
PE-1	$+M_z$	0.250	2.84	0.42		0.52		0.34
PE-2	$-M_z$	0.250	2.84	0.47			0.63	0.30
PE-3	$M_y$	0.250	2.84	0.51			0.56	0.34
PE-4	$+M_z + P$	0.250	2.84	0.30			0.33	0.38
PE-5	$-M_z + P$	0.250	2.84	0.28			0.37	0.40
PE-6	$M_y + P$	0.250	2.84	0.35			0.40	0.39
PE-7	$+M_z$	0.405	2.91	0.35			0.52	0.55
PE-8	$-M_z$	0.405	2.91	0.43			0.49	0.46
PE-9	$M_y$	0.405	2.91	0.44			0.39	0.53
PE-10	$+M_z$	0.167	1.89	0.29			0.57	0.36
PE-11	$-M_z$	0.167	1.89	0.30			0.81	0.35
PE-12	$M_y$	0.167	1.89	0.34			0.65	0.38
PE-13	$+M_z + P$	0.167	1.89	0.18			0.42	0.40
PE-14	$M_y + P$	0.167	1.89	0.22			0.47	0.40
PE-15	$-M_z$	0.250	2.84	0.62	0.22	0.33	0.60	0.23
PE-16	$-M_z$	0.250	2.84	0.64	0.23		0.54	0.22
PE-17	$-M_z$	0.167	1.89	0.38	0.17	0.31	0.41	0.27
PE-18	$-M_z$	0.405	2.91	0.46	0.23	0.30	0.34	0.42
PE-19	$-M_z$	0.167	1.89	0.41		0.34	0.48	0.25
PE-20	$-M_z$	0.270	1.94	0.26		0.36	0.39	0.54

moment for straight pipe. The latter is given by<sup>13</sup>

$$M_0 = \sigma_0 t D^2 \left\{ 1 - \frac{3}{4} \left[ \frac{P(D/2t)}{\sigma_0} \right]^2 \right\}^{1/2},$$

where  $D$  is the mean diameter and  $P$  is the internal pressure.

The first two normalized quantities in Table 8,  $M_{0.2\%}/M^*$  and  $M_{PL}/M^*$ , correspond to reciprocal shape factors (the ratio of the moment at first yield to the fully plastic moment). The shape factor for straight pipe of elastic, perfectly plastic material is  $4/\pi$ . The ratio  $M_{0.2\%}/M^*$  is plotted as a function of  $1/\lambda_2$  in Fig. 35, where a dashed line at  $\pi/4$  has been drawn for reference. Unique correlations are not identifiable from this plot; however, lines which are indicative of fixed  $R/r$  are shown. Both  $\lambda$  and  $R/r$  dependence are indicated; this is also true for the results shown in Fig. 36, where  $M_{DI}/M^*$  is plotted vs  $1/\lambda_2$ . In both figures, the points for combined loading fall below those for single loadings. Beyond these similarities, there is essentially no correspondence between the sets of data in Figs. 35 and 36.

The ratio  $M_{PL}/M^*$  is also dependent on  $R/r$ , but it appears to be independent of  $\lambda$ . Finally,  $M_{SG}/M^*$  does not show a discernible dependence on either parameter.

The experimentally determined shape factor is given by  $M^*/M_{SG}$ , and values obtained range from 2.78 to 3.33. The shape factor for straight pipe, 1.27, is much lower. A second comparison can be made with experimental values obtained by Gross<sup>14</sup> from elbows with dimensions similar to those for specimens PE-1 through -6. In-plane loading corresponding to  $-M_z$  in the present case was used, and ratios of load causing collapse divided by load causing local yielding (as determined by strain gages) were obtained for two 152.4-mm (6-in.) specimens. These values were 2.06 and 2.11 for  $\lambda_2$  values of 0.283 and 0.269, respectively, and  $R/r$  values of 2.85 and 2.84. The strain gages used by Gross were mounted at the  $45^\circ$  plane at  $22.5^\circ$  intervals around the circumference on both the inside and the outside surface of the elbow. Because of the spacing and the long gage length, 20.6 mm (13/16 in.), localized yielding probably was

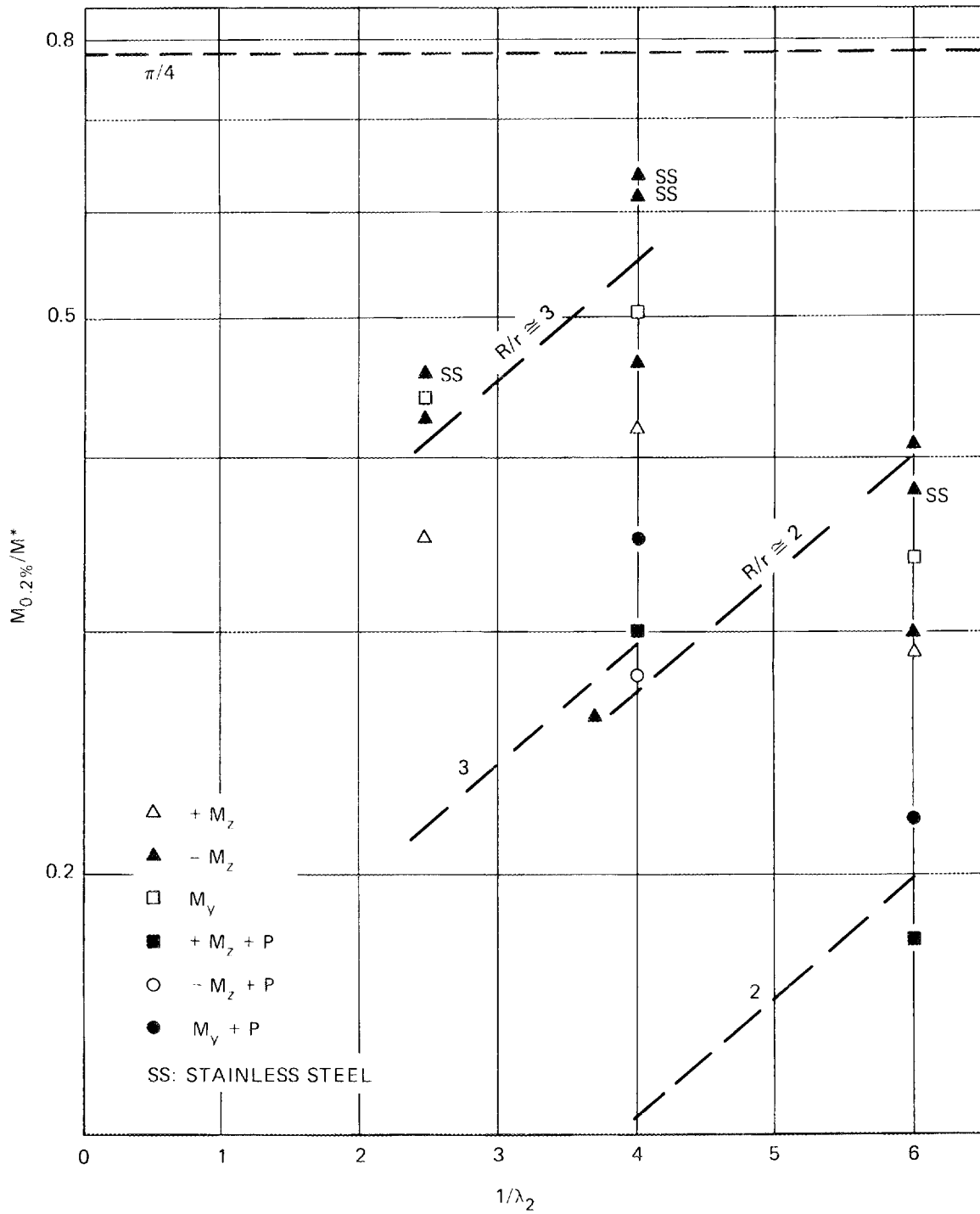


Fig. 35. Calculated moment at onset of yielding.

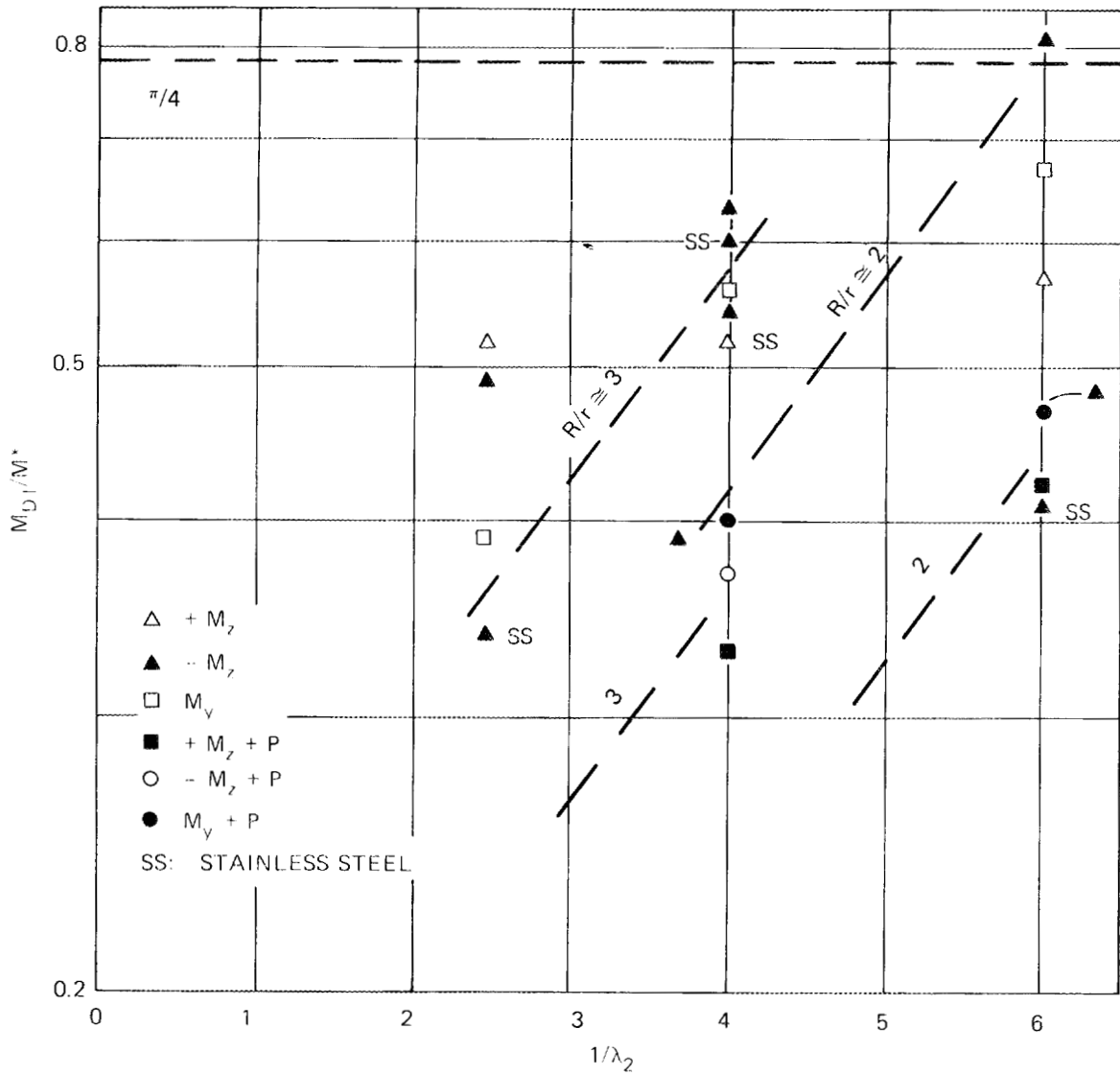


Fig. 36. Moment at onset of nonlinear response as determined from dial-gage readings.

not detected. Hence, the resulting shape factors are low compared to those obtained here; but, altogether, the experimentally determined shape factors from the study by Gross indicate a lack of dependence on  $\lambda$  in concert with the results given in this report.

The results in the last column of Table 8,  $M^*/M_0$ , are plotted vs  $1/\lambda_2$  in Fig. 37, where the specimen number is given at the left of each

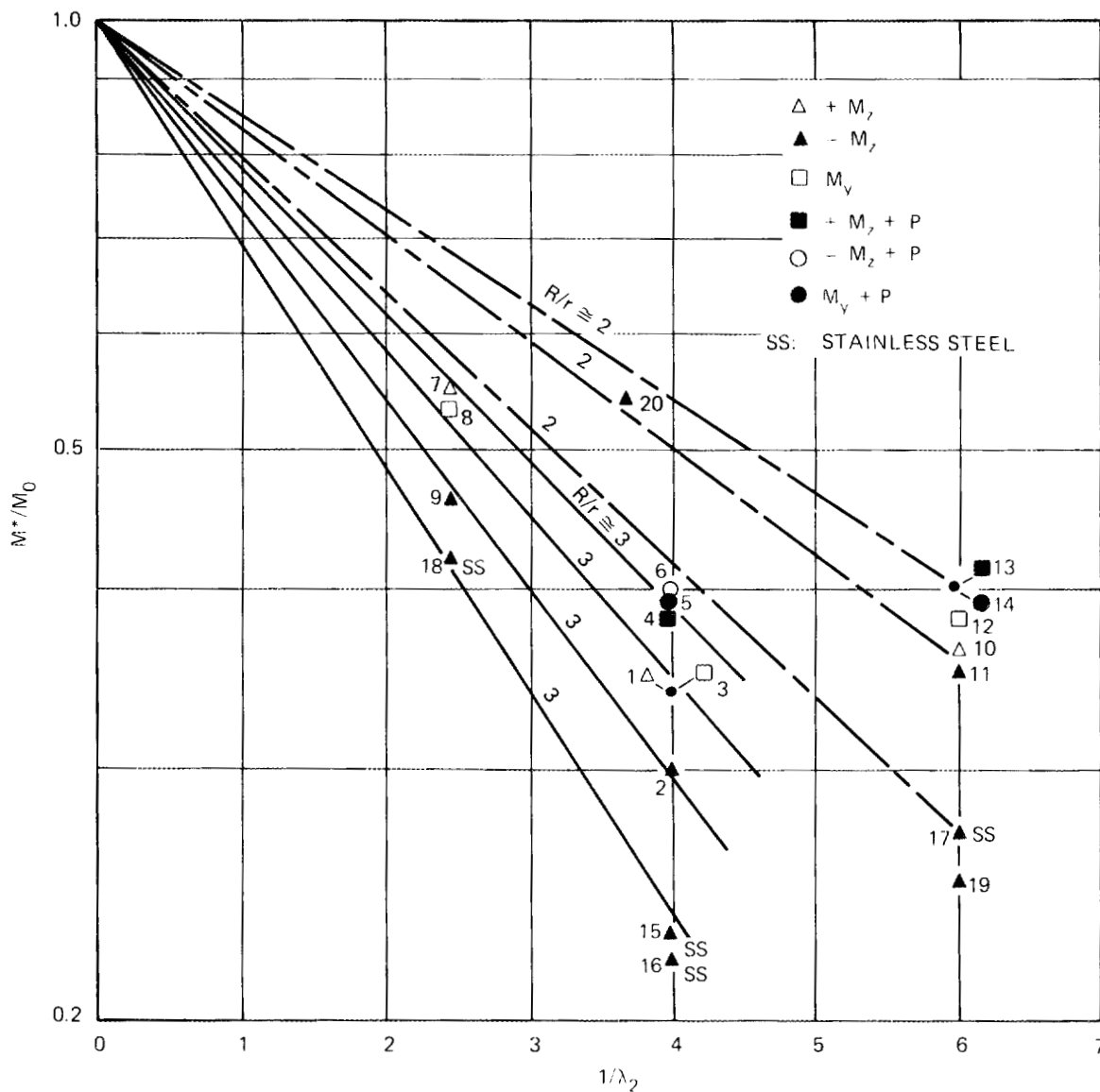


Fig. 37. Normalized plastic collapse moment.

point. By postulating that the results for straight pipe encompass all  $R/r$  values, a fan of straight lines emanating from unity at  $1/\lambda_2 = 0$  has been used for data examination. From Fig. 37, it is seen that the data may be correlated on the basis of  $R/r$  as defined. In addition to  $\lambda$  and  $R/r$  dependence,  $M^*/M_0$  is dependent upon material and loading.

The magnitude of  $M^*/M_0$  decreases as  $R/r$  ratio increases, with the values being lowest for stainless steel. Points for moment loadings

also appear to lie on a single line for  $R/r \cong 2$ . However, when  $R/r \cong 3$ , the results for  $-M_z$  fall below those for  $+M_z$  and  $M_y$ . Combined loadings give higher  $M^*/M_0$  ratios for both  $R/r$  ratios. The value of 0.25 for PE-19 ( $\lambda_2 = 0.167$  and  $R/r = 1.89$ ) is incongruous with the remainder of the data set, but the cause is unknown.

#### CONCLUSIONS

Experimentally determined collapse moments for 20 commercial elbows are presented. The data can be interpreted on an overall basis in terms of the ratios of the calculated maximum elastic bending stresses at collapse to the yield stresses. The trends are identified as follows: For an elbow of given wall thickness, radius, and material under external load alone, the collapse moment is smaller when an in-plane moment ( $-M_z$ ), which tends to cause the bend radius to decrease, is applied than it is for the other two cases of moment loading studied. The addition of internal pressure for this case gives collapse moments for long-radius sched-40 elbows that are greater than the moments for the other two combined loading cases studied for this type of specimen. Internal pressure generally increases the moment at collapse as defined here, although the load at the onset of nonlinear response is decreased. The ratio of calculated stress to yield stress, as defined in the foregoing, increases with increasing wall thickness. Finally, this ratio increases with decreasing bend radius for a given wall thickness.

Additional conclusions are drawn by considering the ratio of the collapse moment to the theoretical collapse moment for straight pipe,  $M^*/M_0$ . These ratios are dependent upon  $\lambda$ ,  $R/r$ , materials, and loading. They decrease with decreasing  $\lambda$  and with increasing  $R/r$  ratio. They also show that the collapse moment is smaller when an in-plane moment, which tends to cause the radius to decrease, is applied. Addition of internal pressure increases the moment ratio; the ratios are less for stainless steel than for carbon steel. Overall, the data show very consistent trends. However, additional studies are required before these results can be considered generally applicable outside the ranges of the parameters examined.

The changes in geometry were generally small, although some ovaling of the cross section occurred in each case. The greatest ovaling occurred in the stainless-steel specimens, giving 9 to 15% ovality after test.

The results show that the collapse moments for the stainless steel elbows became increasingly smaller than those for carbon steel specimens, which were subjected to the same loading conditions and had the same dimensions, for decreases in the parameter  $\lambda$ . Although the yield stress is not the only factor in determining the plastic behavior of a structure, the results obtained in this study indicate that the effective yield stress for stainless steel is significantly lower than the value corresponding to 0.2% offset strain.

#### ACKNOWLEDGMENT

The author acknowledges with appreciation the assistance of E. C. Rodabaugh of Battelle Columbus Laboratories and S. E. Moore of ORNL, who provided guidance in establishing this series of tests and help in interpreting the results. Sincere appreciation is also extended to S. E. Bolt, J. E. Smith, T. G. Hill, J. P. Rudd, and R. Smith of ORNL, who performed the tests; to W. G. Dodge for data processing and for stress and strain computations; and to H. D. Curtis for dimensional data.

#### REFERENCES

1. H. H. Demir and D. C. Drucker, "An Experimental Study of Cylindrical Shells Under Ring Loading," pp. 205-20 in *Progress in Applied Mechanics (The Prager Anniversary Volume)*, Macmillan, New York, 1963.
2. S. E. Bolt and W. L. Greenstreet, "Experimental Determinations of Plastic Collapse Loads for Pipe Elbows," ASME Paper 71-PVP-37, 1971.
3. J. P. DenHartog, *Advanced Strength of Materials*, pp. 234-45, McGraw-Hill, New York, 1952.
4. W. L. Greenstreet, S. E. Moore, and R. C. Gwaltney, "Progress Report on Studies in Applied Solid Mechanics," ORNL-4576 (August 1970).

5. R. M. Haythornthwaite, "A More Rational Approach to Strain Hardening Data," pp. 201-18 in *Engineering Plasticity*, ed. by J. Heyman and F. A. Leckie, Cambridge University Press, London, 1968.
6. G. Augusti and S. d'Agostino, "Experiments on the Plastic Behavior of Short Steel Cylindrical Shells Subject to Internal Pressure," pp. 45-47 in *Pressure Vessel Technology Part I*, American Society of Mechanical Engineers, New York, 1969.
7. Fernand Ellyin, "Elastic-Plastic Behavior of Intersecting Shells," *J. Eng. Mech. Div., ASCE*, 95, 69-94 (February 1969).
8. J. Schroeder, K. R. Srinivasaiah, and P. Graham, "Analysis of Test Data on Branch Connections Exposed to Internal Pressure and/or External Couples," *Weld. Res. Counc. Bull.* 200 (November 1974).
9. Fernand Ellyin, "Experimental Investigation of Limit Loads of Nozzles in Cylindrical Vessels," *Weld. Res. Counc. Bull.* 219 (September 1976).
10. Fernand Ellyin, "An Experimental Study of Elastic-Plastic Response of Branch Pipe Tee Connections Subjected to Internal Pressure, External Couples and Combined Loadings," *Weld. Res. Counc. Bull.* 230 (September 1977).
11. S. Palusamy, "Influence of External Loads on Pressure-Carrying Capacity of Outlet Connections," *ASME Trans., Ser. B, J. Eng. Ind.* 95(1), 113-20 (February 1973).
12. W. G. Dodge and S. E. Moore, "Stress Indices and Flexibility Factors For Moment Loadings on Elbows and Curved Pipe," *Weld. Res. Counc. Bull.* 179 (December 1972).
13. E. C. Rodabaugh, "Interpretive Report on Limit Analysis and Plastic Behavior of Piping Products," Report Submitted to PVRC Design Division, Task Group on Characterization of Plastic Behavior of Structures, September 1976.
14. N. Gross, "Experiments on Short-Radius Pipe Bends," *Proceedings of Institute of Mechanical Engineers* 166(A), 406 (1952).



## Appendix

## DIMENSIONAL DATA FOR SPECIMENS PE-17 THROUGH -20

Dimensional data were obtained prior to and following test completion for specimens PE-17 and -20; specimens PE-18 and -19 were measured after testing only. The outside diameters (OD) and thicknesses (T) are listed in Table A-1 together with the locations at which these measurements were taken. Also listed are the ovalities, which ranged from a maximum of 1.3% (prior to test) to 14.5% (following test). The thickness deviations ranged from 0.0 to 14.2% of nominal for PE-17; -7.4 to +22% for PE-18; -10 to +7.9% for PE-19%; and -11.6 to +10.2% for PE-20. All elbow dimensions are within limits given by the applicable manufacturing standard.

Table A-1. Measured specimen dimensions<sup>a</sup>

Specimen No.	Location		OD (in.)		Location angle	T (in.)	Ovality <sup>d</sup> (%)	
	Plane <sup>b</sup>	Angle <sup>c</sup>	Pretest	Posttest			Posttest	Pretest
PE-17	A	0-180	6.700	6.488	0	0.295	0.6	5.4
		90-270	6.660	6.848	90	0.332		
					180	0.296		
					270	0.307		
	Mid	0-180	6.575	6.332	0	0.250	0.7	9.3
		90-270	6.622	6.937	90	0.288		
					180	0.316		
					270	0.278		
	L	0-180	6.700	6.460	0	0.290	1.1	4.7
		90-270	6.625	6.773	90	0.298		
					180	0.301		
					270	0.303		
PE-18	A	0-180		6.423	0	0.471		5.1
		90-270		6.758	90	0.477		
					180	0.467		
					270	0.501		
	Mid	0-180		6.105	0	0.400		14.5
		90-270		7.064	90	0.459		
					180	0.514		
					270	0.434		
	L	0-180		6.470	0	0.514		4.2
		90-270		6.748	90	0.525		
					180	0.455		
					270	0.494		
PE-19	A	0-180		6.432	0	0.252		5.9
		90-270		6.820	90	0.293		
					180	0.285		
					270	0.281		
	Mid	0-180		6.412	0	0.252		7.6
		90-270		6.920	90	0.290		
					180	0.269		
					270	0.270		
	L	0-180		6.471	0	0.260		5.6
		90-270		6.845	90	0.273		
					180	0.252		
					270	0.302		
PE-20	A	0-180	6.640	6.352	0	0.386	0.4	8.2
		90-120	6.655	6.898	90	0.458		
					180	0.443		
					270	0.450		
	Mid	0-180	6.566	6.199	0	0.383	1.3	12.6
		90-120	6.653	7.035	90	0.437		
					180	0.423		
					270	0.440		
	L	0-180	6.624	6.410	0	0.382	0.4	6.3
		90-120	6.647	6.824	90	0.450		
					180	0.383		
					270	0.457		

<sup>a</sup> 1 in. = 25.4 mm.

<sup>b</sup> A = fixed end; Mid = 45° plane; L = loaded end.

<sup>c</sup> Angular locations correspond to those in Figs. 7 and 8.

$$d\% \text{ ovality} = \frac{OD_{\max} - OD_{\min}}{OD_{\text{av}}} \times 100.$$

## INTERNAL DISTRIBUTION

- |        |                   |        |                               |
|--------|-------------------|--------|-------------------------------|
| 1.     | B. R. Bass        | 39.    | M. Levenson                   |
| 2.     | R. L. Battiste    | 40.    | K. C. Liu                     |
| 3.     | M. Bender         | 41.    | R. E. MacPherson              |
| 4.     | J. J. Blass       | 42.    | W. J. McAfee                  |
| 5.     | S. E. Bolt        | 43.    | J. G. Merkle                  |
| 6.     | R. H. Bryan       | 44.    | J. L. Mershon (consultant)    |
| 7.     | J. W. Bryson      | 45-64. | S. E. Moore                   |
| 8.     | J. R. Buchanan    | 65.    | F. R. Mynatt                  |
| 9.     | J. H. Butler      | 66.    | C. B. Oland                   |
| 10.    | J. P. Callahan    | 67.    | T. W. Pickeel                 |
| 11.    | C. J. Claffey     | 68.    | H. Postma                     |
| 12.    | J. A. Clinard     | 69.    | C. E. Pugh                    |
| 13.    | C. W. Collins     | 70.    | M. Richardson                 |
| 14.    | W. E. Cooper      | 71.    | D. N. Robinson                |
| 15.    | J. M. Corum       | 72.    | M. R. Sheldon                 |
| 16.    | W. B. Cottrell    | 73.    | G. C. Smith                   |
| 17.    | T. J. Delph       | 74.    | J. E. Smith                   |
| 18.    | W. G. Dodge       | 75.    | I. Spiewak                    |
| 19.    | M. H. Fontana     | 76.    | W. C. T. Stoddart             |
| 20.    | W. R. Gall        | 77.    | R. E. Textor                  |
| 21-30. | W. L. Greenstreet | 78.    | H. E. Trammell                |
| 31.    | R. C. Gwaltney    | 79.    | D. B. Trauger                 |
| 32.    | J. F. Harvey      | 80.    | G. D. Whitman                 |
| 33.    | R. W. Henderson   | 81.    | G. T. Yahr                    |
| 34.    | R. F. Hibbs       | 82.    | ORNL Patent Office            |
| 35.    | S. K. Iskander    | 83-85. | Central Research Library      |
| 36.    | W. G. Johnson     | 86.    | Document Reference Section    |
| 37.    | M. A. Karnitz     | 87-92. | Laboratory Records Department |
| 38.    | P. R. Kasten      | 93.    | Laboratory Records, ORNL-RC   |

Subcontractors

- 94-95. G. A. Greenbaum, Mechanics Research, Inc., Santa Monica, CA  
90406
- 96-97. N. E. Johnson, Mechanics Research, Inc., Oak Ridge, TN 37830
- 98-99. E. C. Rodabaugh, Battelle-Columbus Laboratories, Columbus, OH  
43201

## EXTERNAL DISTRIBUTION

- 100-107. Director, Office of Nuclear Regulatory Research, NRC, Washington, D.C. 20555
- 108. Director, Reactor Division, DOE, ORO
- 109. Research and Technical Support Division, DOE, ORO
- 110-194. Design Criteria for Piping and Nozzles Program Distribution
- 195-498. Given distribution as shown under category NRC-5 (25 copies --- NTIS)